



Cite this: *EES Batteries*, 2025, **1**, 1083

## K–O<sub>2</sub> batteries: overcoming challenges & unlocking potential

Divyaratan Kumar,<sup>a,b</sup> K Brijesh,<sup>c</sup> Kalleshappa Bindu,<sup>d</sup> Basharat Ramzan,<sup>e</sup> Surender Kumar \*<sup>e</sup> and Ziyauddin Khan \*<sup>a,b</sup>

Batteries have long been a cornerstone of energy storage technologies, offering low-carbon and sustainable solutions across diverse applications from large-scale power grids to electric vehicles and portable electronics. In response to growing global energy demands, research efforts are increasingly directed toward advancing battery chemistries and cell designs to achieve higher performance, efficiency, and scalability. Among emerging systems, potassium–oxygen (K–O<sub>2</sub>) batteries have attracted significant attention due to their high theoretical energy density (~935 Wh kg<sup>-1</sup>) and the Earth-abundant nature of potassium. This review presents a comprehensive overview of K–O<sub>2</sub> battery technology, covering fundamental operating principles, key performance limitations, and persistent challenges. Particular focus is given to critical aspects such as electrode architecture, electrolyte stability, and oxygen-related electrochemistry, which collectively govern cell efficiency and durability. In addition, we highlight recent advancements aimed at overcoming these barriers and provide a critical assessment of the current technological readiness of K–O<sub>2</sub> batteries. While the system holds considerable promise, substantial progress is still required to translate laboratory success into practical, real-world applications. Finally, future directions and opportunities for the development and integration of K–O<sub>2</sub> batteries are discussed.

Received 3rd July 2025,  
Accepted 27th July 2025

DOI: 10.1039/d5eb00122f

[rsc.li/EESBatteries](http://rsc.li/EESBatteries)

### Broader context

Metal–O<sub>2</sub> batteries are an attractive technology primarily due to their high specific energy. Li–O<sub>2</sub> batteries, for instance, offer the highest theoretical specific energy (~12 kWh kg<sup>-1</sup>), which is comparable to that of gasoline (~13 kWh kg<sup>-1</sup>), making them a promising option for grid and stationary storage applications. However, Li–O<sub>2</sub> batteries suffer from poor efficiency (<60%) and limited rechargeability. In contrast, K–O<sub>2</sub> batteries have demonstrated an energy efficiency of over 90% without the need for an electrocatalyst. This review explores advancements in K–O<sub>2</sub> batteries, covering research on the anode, electrolyte, and electrocatalyst. Additionally, it addresses a key question: “Why does this technology require focused research?”

## 1. Introduction

Fossil fuels are an inexpensive and readily available energy source commonly employed to power vehicles. However, the uninterrupted consumption of fuels and the never-ending energy demand bring us to the verge of consuming all the fossil fuel resources.<sup>1,2</sup> Additionally, there is a climate issue associated with the usage of fossil fuels, which has forced

researchers globally to find an environmentally friendly and cost-effective energy source. To combat the climate change associated with fossil fuels, electrochemical energy storage devices were regarded as a potential alternative.<sup>3</sup> Two kinds of electrochemical energy storage devices have been known: one is supercapacitors and the other is batteries. Supercapacitors are regarded as power devices, which make the usage of batteries as energy devices advantageous, as they can provide a continuous energy supply on demand.<sup>4</sup> The oil crisis in the 1970s led Prof. Stanley Whittingham, working for ExxonMobil, to explore the possibility of developing Li-ion batteries (LIBs) to get rid of fossil fuels.<sup>5</sup> Though the electrochemical properties of lithium were reported in early 1913,<sup>6</sup> it took more than 50 years to explore the feasibility of LIBs. Further developments made by Prof. John B. Goodenough and Prof. Akira Yoshino inspired Sony and Asahi Kasei teams led by Nishi to successfully commercialize LIBs in 1991. Afterwards, the application of LIBs was found in most of the electronic portable

<sup>a</sup>Laboratory of Organic Electronics, Department of Science and Technology, Linköping University, Norrköping, SE-601 74, Sweden.  
E-mail: ziyauddin.khan@liu.se

<sup>b</sup>Wallenberg Wood Science Center, ITN, Linköping University, Norrköping, Sweden

<sup>c</sup>Department of Physics, National Institute of Technology Karnataka, P.O. Srinivasnagar, Surathkal, Mangaluru 575 025, India

<sup>d</sup>Department of Inorganic and Physical Chemistry, Indian Institute of Science, Bangalore – 560012, India

<sup>e</sup>CSIR – Advanced Materials and Processes Research Institute (AMPRI), Bhopal – 462026, India. E-mail: surender@ampri.res.in



devices and household appliances. Despite the emergence of newer battery technologies, LIBs remain dominant in the electronic gadget market due to their high specific energy density of 100–250 Wh kg<sup>-1</sup>, low density of lithium (0.534 g cm<sup>-3</sup>), and low standard reduction potential of lithium (-3.04 V vs. SHE).<sup>7</sup> Despite their widespread use, the energy density of LIBs remains a limiting factor for their application in electric vehicles (EVs) and hybrid electric vehicles (HEVs), as it typically ranges from 100 to 250 Wh kg<sup>-1</sup>, which is considered insufficient.<sup>8</sup> Scientists have turned their attention towards metal–air batteries, including those based on Li, Na, K, Mg, Al, Zn, and Fe due to their impressive specific energy, volumetric energy, and cell voltage, as demonstrated in Fig. 1.<sup>9,10,11–13</sup> While researchers have investigated numerous metals from the periodic table for battery applications, alkali metals such as Li, Na, and K offer distinct advantages over other metals in terms of energy density, reaction kinetics, and cost. In this context, metal–oxygen batteries, such as Li–O<sub>2</sub>,<sup>11</sup> Na–O<sub>2</sub>,<sup>10</sup> and K–O<sub>2</sub> batteries,<sup>14</sup> are gaining attention from scientists. The physical properties of the alkali metals (Li, Na and K)<sup>15,16</sup> are listed in Table 1, which compares Li, Na, and K in terms of their atomic number, natural abundance in the Earth's crust (ppm), electronic configuration, density, ionic radius, and standard reduction potential.

In particular, Li–O<sub>2</sub> has been sought as a potential candidate for EVs as it provides comparable theoretical specific energy (11 680 Wh kg<sup>-1</sup>) to gasoline.<sup>19</sup> The chemistry of the Li–O<sub>2</sub> battery involves the reaction of metallic Li with oxygen, which yields ~2.96 V cell potential and forms lithium peroxide (Li<sub>2</sub>O<sub>2</sub>) as a discharge product *via* a two-electron process. The main challenges associated with Li–O<sub>2</sub> batteries are the instability of the electrolyte, poor specific capacity, and low round-trip efficiency<sup>20</sup> owing to the sluggish kinetics associated with the Li<sub>2</sub>O<sub>2</sub> formation and blockage of oxygen diffusion pathways of the air electrode arising from the excessive growth of discharge products (Li<sub>2</sub>O<sub>2</sub>).<sup>21</sup> It was also found that the cycling stability of the battery degraded rapidly due to the generation of singlet oxygen (<sup>1</sup>O<sub>2</sub>).<sup>22</sup> Additionally, there are safety and environmental concerns which also limit its large-scale manufacturing.<sup>23</sup> Therefore, searching for a solution beyond Li-based technologies is highly desirable.

Superoxide-based Na–O<sub>2</sub> (1105 Wh kg<sup>-1</sup> of theoretical specific energy based on the NaO<sub>2</sub> discharge product)<sup>24</sup> and K–O<sub>2</sub> (935 Wh kg<sup>-1</sup> of theoretical specific energy based on the KO<sub>2</sub> discharge product)<sup>25</sup> batteries could be possible alternatives to Li–O<sub>2</sub> (3500 Wh kg<sup>-1</sup> of specific energy based on the Li<sub>2</sub>O<sub>2</sub> discharge product).<sup>26,27</sup> The formation of sodium superoxide (NaO<sub>2</sub>) and potassium superoxide (KO<sub>2</sub>) involves one



Fig. 1 Theoretical energy density, specific energy and cell voltage of various metal–air batteries. Reproduced with permission from ref. 17. Copyright 2016 WILEY–VCH Verlag GmbH & Co. KGaA, Weinheim.

Table 1 Comparison of alkali metals relevant to battery applications<sup>8,18</sup>

| Alkali metals | Atomic number | Natural abundance (ppm) | Electronic shell structure | Density (g cm <sup>-3</sup> ) | Ionic radius (Å) | Reduction potential (V) |
|---------------|---------------|-------------------------|----------------------------|-------------------------------|------------------|-------------------------|
| Lithium (Li)  | 3             | 18                      | (2, 1)                     | 0.535                         | 0.76             | -3.04                   |
| Sodium (Na)   | 11            | 22 700                  | (2, 8, 1)                  | 0.968                         | 1.02             | -2.71                   |
| Potassium (K) | 19            | 21 000                  | (2, 8, 8, 1)               | 0.858                         | 1.38             | -2.93                   |



electron transfer, which improves the sluggish kinetics associated with oxygen reduction and oxygen evolution reactions, thereby improving the round-trip efficiency and cycling stability compared to Li–O<sub>2</sub> batteries, where the discharge reaction occurred through 2-electron processes.<sup>28</sup> However, the formation of NaO<sub>2</sub> in non-aqueous media is kinetically preferred but not a thermodynamically stable discharge product. Therefore, NaO<sub>2</sub> further converts into Na<sub>2</sub>O<sub>2</sub> (sodium peroxide) either *via* a disproportionation reaction (2NaO<sub>2</sub> → Na<sub>2</sub>O<sub>2</sub> + O<sub>2</sub>) or an electrochemical reduction reaction (NaO<sub>2</sub> + Na<sup>+</sup> + e<sup>−</sup> → Na<sub>2</sub>O<sub>2</sub>), leading to low cell reversibility.<sup>29</sup> Moreover, recent studies also showed that the formation of singlet oxygen could be a possible reason for the performance degradation in Na–O<sub>2</sub> cells.<sup>30</sup> In contrast to Na–O<sub>2</sub> batteries, KO<sub>2</sub> as the discharge product in non-aqueous K–O<sub>2</sub> batteries is both thermodynamically stable and kinetically preferred which makes K–O<sub>2</sub> an advantageous battery system.<sup>25,31</sup> The fast O<sub>2</sub>/KO<sub>2</sub> redox couple guarantees low polarization and also enables the rechargeability of the cell below 3 V vs. K/K<sup>+</sup>, thus significantly minimizing the formation of singlet oxygen (as is the case for both Li–O<sub>2</sub> and Na–O<sub>2</sub> batteries).<sup>14</sup> Moreover, since the rechargeability can be achieved below 3 V vs. K/K<sup>+</sup>, this avoids the participation of a parasitic reaction, which typically occurs at higher potentials,<sup>28</sup> thereby exhibiting high round-trip efficiency (>90%). Additionally, K has a higher abundance in the Earth's crust that can also play a vital role,<sup>32</sup> thereby making K–O<sub>2</sub> batteries a potential alternative to Li–O<sub>2</sub> batteries. The development of this technology is at an early stage and requires more in-depth investigation about electrode/electrolyte interfaces, their effect on reaction kinetics and safety issues. This review emphasizes the key aspects of durability and recyclability for battery applications with special reference to the challenges involved therein. A detailed discussion on basic cell design, reaction mechanisms, novel anode and cathode materials used and their effect on performance is provided. It concludes with a critical outlook on future research directions and practical advancements in the field of K–O<sub>2</sub> batteries.

## 2. Cell design and reaction mechanisms for metal–air and K–O<sub>2</sub> batteries

### 2.1 Cell reaction of the metal–air battery

Before starting the description, it would be worth mentioning that a metal–air battery refers to a system that uses air as the source of oxygen, while a metal–O<sub>2</sub> battery refers to a system that uses pure oxygen as the source of oxygen.

Metal–air batteries have not been discovered recently; in fact, the primary Zn–air battery (typically called Zn–air as it utilises air as a source of oxygen) was first constructed in 1878 and was commercialised in 1932 before the existence of LIBs.<sup>33</sup> In general, metal–O<sub>2</sub> batteries are electrochemical cells which are powered by the oxidation of metal and the reduction

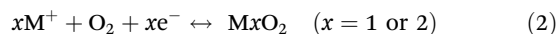
of oxygen *via* the oxygen reduction reaction (ORR).<sup>34</sup> In a typical design, a metal–O<sub>2</sub> battery consists of a metal electrode as anode, an air cathode commonly known as the electrocatalyst (counter electrode), oxygen/air as the cathode and a suitable electrolyte. Alkali metals (Li, Na and K),<sup>35–37</sup> alkaline earth metals (Mg and Ca)<sup>38,39</sup> and first-row transition metals (such as Fe and Zn)<sup>40,41</sup> can be used as metal anodes for metal–O<sub>2</sub>/air batteries. However, electrolyte selection depends on the nature and properties of the metal anode (in Li, Na and K cases, preferably non-aqueous)<sup>40,41</sup> and cell configuration.<sup>8</sup> The air-breathing cathode should have a porous nature that continuously permits gas flow either from the surrounding air or from an oxygen tank. The basic design of any metal–O<sub>2</sub>/air batteries combines both fuel cells and conventional metal-ion batteries. A schematic diagram of metal–O<sub>2</sub>/air batteries,<sup>42,43</sup> whether non-aqueous or aqueous, is shown in Fig. 2. During discharge of a metal–O<sub>2</sub>/air battery, metal at the negative electrode gets oxidized and generates an electron which moves to the counter electrode (air electrode) where it combines with the oxygen, which gets reduced *via* the ORR. During charging, the metal ion gets deposited on the negative electrode, and oxygen evolution takes place at the air electrode. Based on the electrolyte, the electrochemical reactions in the cell differ considerably; therefore, the discharge products are also different in non-aqueous and aqueous electrolytes. The involved electrochemical reactions occurring in both electrodes in aqueous and non-aqueous electrolytes are presented below:<sup>43</sup>

#### In a non-aqueous electrolyte

At the negative electrode:



At the air electrode:



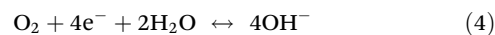
#### In an aqueous electrolyte

At the negative electrode:

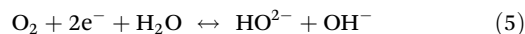


At the air electrode:

4e<sup>−</sup> transfer pathway<sup>44</sup>



2e<sup>−</sup> transfer pathway<sup>45,46</sup>



Metals such as Zn, Fe or Mg can be directly used in aqueous medium, though these metals are thermodynamically unstable and reduce water to produce hydrogen. However, the overpotential for hydrogen reduction can be increased by using various strategies such as using alloyed anodes, passivating the surface of metals or modifying the electrolyte, such as water-in-salt electrolyte.<sup>47</sup> In contrast, Li, Na and K metals react violently with water; therefore, they cannot be directly used in aqueous electrolytes. Hence, for the operation of these



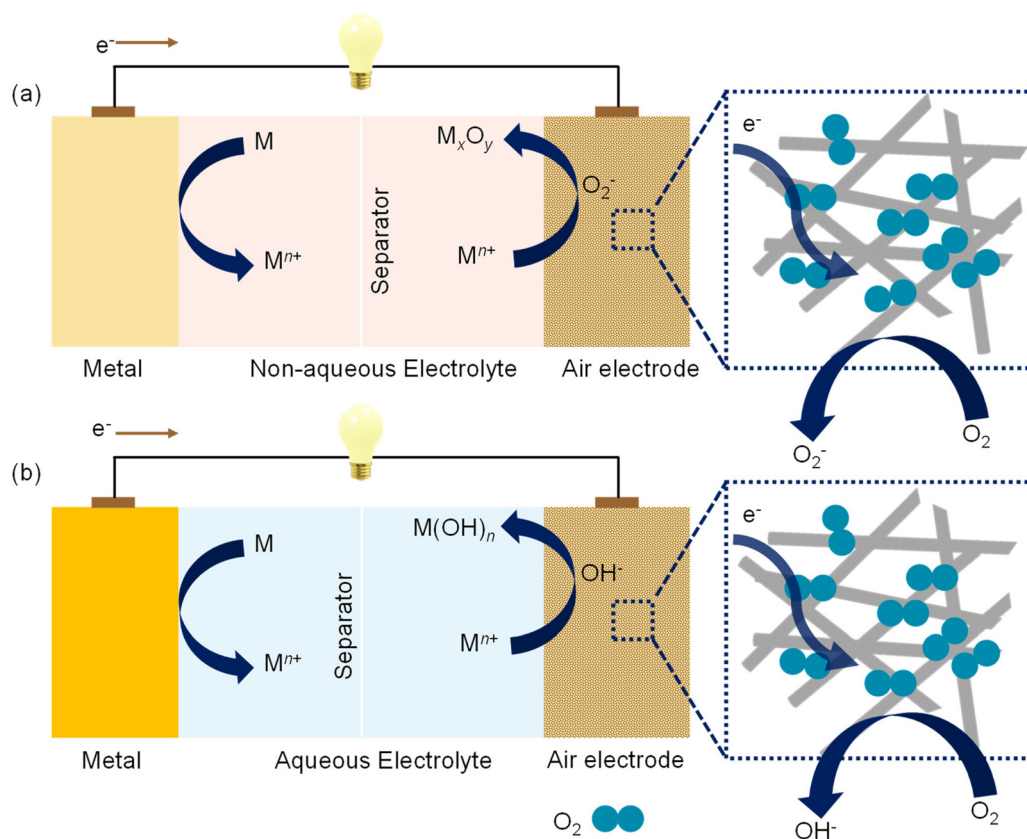


Fig. 2 Schematic illustration of (a) a metal–O<sub>2</sub> cell in a non-aqueous system and (b) metal–air cell with aqueous electrolyte.

metals with aqueous electrolytes, the metallic anode is usually protected by an ionic conductive ceramic film known as a solid electrolyte membrane.<sup>48</sup> This solid electrolyte only allows passage of metal ions from the aqueous electrolyte to the negative electrode while blocking water.<sup>49</sup> The advantage of aqueous electrolytes is the formation of highly water-soluble discharge products that can avoid the clogging issues (thereby improving the round-trip efficiency and cycling stability) related to the air electrode in non-aqueous electrolyte. Despite this benefit, the cell design of these metal-based aqueous batteries is more complicated and requires additional steps, which eventually makes it challenging for large-scale applications.

While it may be easier to prepare batteries using non-aqueous systems than aqueous ones using alkali metals, their performance is often compromised due to the accumulation of insoluble discharge products that can block the pores of the air electrode. This can lead to poor round-trip efficiency and cycling stability. In addition, the air electrode requires a membrane which should block moisture and CO<sub>2</sub> from ambient air and only allow passage of O<sub>2</sub>. Using this kind of membrane will increase the fabrication cost of the cell, which can pose a significant hurdle for practical application. Therefore, it is reasonable to conclude that both types of cells present distinct advantages and limitations, warranting targeted research to overcome their respective challenges.

## 2.2 Cell components of metal–O<sub>2</sub> batteries

Both metal–O<sub>2</sub> and metal–air batteries typically consist of three main components: an anode, an air cathode, and an electrolyte. The anode is usually made of a metal that can undergo oxidation, such as Li, Na, K or Zn. The air cathode is composed of a porous material that allows oxygen to enter and participate in electrochemical reactions.<sup>50</sup> Common air cathode materials include carbon,<sup>51,52</sup> precious metals with carbon,<sup>53,54</sup> metal oxides,<sup>55,56</sup> and perovskite-type materials.<sup>57</sup> The cathode of a metal–O<sub>2</sub> battery typically consists of a metallic current collector, a gas diffusion layer, and a coated catalyst. The gas diffusion layer (GDL) serves multiple critical functions: it provides mechanical support for the catalyst layer, enables efficient oxygen transport to the reaction sites, and acts as a barrier to prevent the intrusion of moisture, carbon dioxide, and other contaminants into the battery. A thin, lightweight, porous, and hydrophobic gas diffusion layer effectively bridges the catalyst and oxygen. Additionally, it provides a hydrophobic barrier to prevent electrolyte leakage while maintaining hydrophilic microchannels for enhanced catalytic activity (Fig. 2b).<sup>15,58</sup> A bifunctional catalytic layer is essential at the cathode to improve both the ORR and the oxygen evolution reaction (OER), as oxygen kinetics are inherently slow. Unlike conventional metal-ion batteries, metal–O<sub>2</sub> batteries utilize oxygen directly from the supply.<sup>59</sup> The electrolyte plays



a crucial role in ion transport between the anode and cathode. It must be compatible with the metal anode and cathode materials while providing sufficient ionic conductivity. Solid-state electrolytes are particularly attractive for metal–O<sub>2</sub> batteries due to their enhanced stability and safety compared to liquid electrolytes.<sup>43</sup>

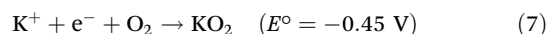
### 2.3 Cell design and reaction mechanism of the K–O<sub>2</sub> battery

Research on K-metal-based batteries has gained momentum, with early work by Eftekhari *et al.* in 2004 on K-ion batteries inspiring further exploration of these energy systems.<sup>23</sup> This progress led to the development of the first low-overpotential K–O<sub>2</sub> battery by Ren *et al.* in 2013, where K<sup>+</sup> ions captured O<sub>2</sub><sup>−</sup> to form the thermodynamically stable KO<sub>2</sub> as the discharge product.<sup>25</sup> The cell design of a K–O<sub>2</sub> battery consists of a K metal anode, a separator with an aprotic electrolyte and an air electrode connected with an oxygen reservoir (Fig. 3a). Similarly, its cell chemistry involves plating/stripping of K metal at the anode and OER/ORR at the air cathode as presented in eqn (6)–(8).

Anode half-cell reaction:



Cathode half-cell reaction:



Overall cell reaction:



In Li–O<sub>2</sub> batteries with aprotic electrolytes, the reduction of oxygen and reaction of reduced oxygen with Li<sup>+</sup> ions forms LiO<sub>2</sub>, a kinetically favoured intermediate that undergoes disproportionation (2LiO<sub>2</sub> → Li<sub>2</sub>O<sub>2</sub> + O<sub>2</sub>) or electrochemical reduction (LiO<sub>2</sub> + Li<sup>+</sup> + e<sup>−</sup> → Li<sub>2</sub>O<sub>2</sub>), to form thermodynamically stable Li<sub>2</sub>O<sub>2</sub> which is a two-electron process. Na- and K-metal-based technologies are considered promising alternatives to Li-based systems, owing to their comparable electrochemical properties, greater elemental abundance, and

lower material cost. In the case of aprotic Na–O<sub>2</sub> batteries, NaO<sub>2</sub> and Na<sub>2</sub>O<sub>2</sub> formations have been reported, with Na<sub>2</sub>O<sub>2</sub> being thermodynamically favoured, while NaO<sub>2</sub> is the kinetically preferred discharge product.<sup>61</sup> However, no conclusive evidence confirms either as the predominant discharge product.<sup>8</sup> In contrast to both (Li–O<sub>2</sub> and Na–O<sub>2</sub>), KO<sub>2</sub> is the sole discharge product in non-aqueous K–O<sub>2</sub> batteries, as it is both thermodynamically stable and kinetically preferred (Table 2 compares different alkali metals and their electrochemical reactions, discharge products, number of electrons transferred, cell voltage theoretical specific energy and Gibbs free energy), making K–O<sub>2</sub> batteries an advantageous system (as shown in Fig. 3b) as K–O<sub>2</sub> battery operates through a one-electron redox process *via* the O<sub>2</sub>/O<sub>2</sub><sup>−</sup> redox couple. Due to this reason, an effective solution to the persistent kinetic challenges of ORR/OER in oxygen batteries can be achieved without relying on high-performance electrocatalysts.<sup>60</sup> Non-aqueous K–O<sub>2</sub> batteries operate with below 50 mV potential gap at modest current densities lower than that of aprotic Li–O<sub>2</sub> batteries (Fig. 3c), achieving >90% round-trip efficiency due to fast charge transfer kinetics and low overpotentials.<sup>10,25</sup> The significantly reduced charging overpotential and high round-trip efficiency are due to the comparable O–O bond lengths in O<sub>2</sub><sup>−</sup> (0.128–0.133 nm) and O<sub>2</sub> (0.121 nm), in contrast to O<sub>2</sub><sup>2−</sup> (~0.149 nm). This suggests a lower reorganization energy and a reduced energy barrier for KO<sub>2</sub> to O<sub>2</sub> conversion, as explained by Marcus theory.<sup>62</sup>

### 2.4 Side reactions in K–O<sub>2</sub> batteries and stability of the KO<sub>2</sub> discharge product

Though there have been advantages, the side reactions such as corrosion of the K metal stimulated by the decomposition of electrolyte and oxygen crossover are the primary reasons for the failure of K–O<sub>2</sub> batteries.<sup>63</sup> In K–O<sub>2</sub> batteries, ether-based electrolytes are commonly used, where the oxygen in ether has a chelating ability with metal ions, leading to metal dissolution and consumption. Another issue is the crossover of O<sub>2</sub> from the cathode to the K metal, where it reacts with the K

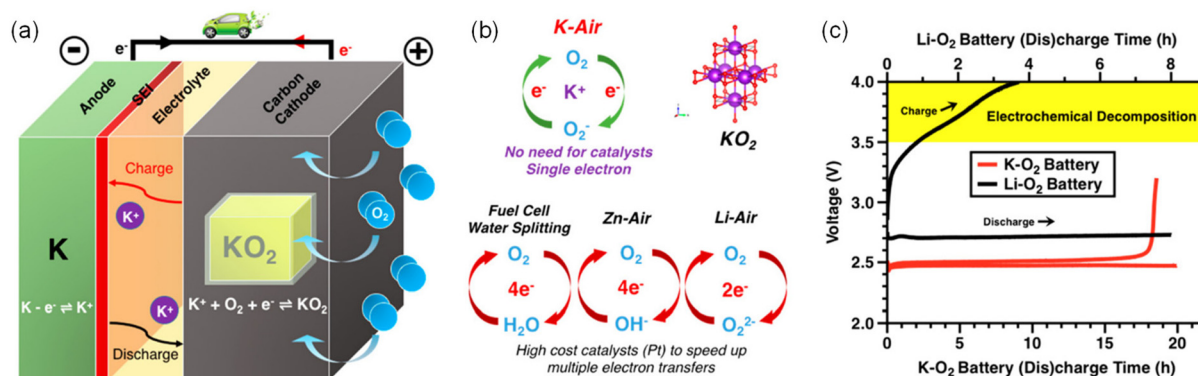


**Fig. 3** (a) Schematic illustration of a K–O<sub>2</sub> battery and the discharge process in K–O<sub>2</sub> batteries. (b) Oxygen redox reaction in fuel cell water splitting, Zn–air, Li–air and K–air batteries. (c) Comparative charge–discharge profiles of Li–O<sub>2</sub> and K–O<sub>2</sub> batteries showing the low overpotentials associated with the charge–discharge process for K–O<sub>2</sub> batteries. Reproduced with permission from ref. 60. Copyright 2018 American Chemical Society.



**Table 2** Electrochemical reactions involved in various aprotic alkali metal–O<sub>2</sub> and metal–air batteries

| Battery           | Overall cell reaction                                 | Discharge product              | Number of electrons transferred | Cell voltage (V) | Theoretical specific energy (Wh kg <sup>-1</sup> ) | $\Delta G$ (kJ mol <sup>-1</sup> ) |
|-------------------|---|--------------------------------|---------------------------------|------------------|--|------------------------------------|
| Li–O <sub>2</sub> | 2Li + O <sub>2</sub> → Li <sub>2</sub> O <sub>2</sub> | Li <sub>2</sub> O <sub>2</sub> | 2                               | 2.96             | 3458   | –570.8                             |
| Li–air            | Li + 0.5H <sub>2</sub> O + 0.25O <sub>2</sub> → LiOH  | LiOH                           | 1                               | 3.45             | 3860 <sup>a</sup><br>5796 <sup>b</sup>             | –332.8                             |
| Na–O <sub>2</sub> | 2Na + O <sub>2</sub> → Na <sub>2</sub> O <sub>2</sub> | Na <sub>2</sub> O <sub>2</sub> | 2                               | 2.33             | 1605   | –449.7                             |
|                   | Na + O <sub>2</sub> → NaO <sub>2</sub>                | NaO <sub>2</sub>               | 1                               | 2.27             | 1108   | –218.8                             |
| Na–air            | Na + 0.5H <sub>2</sub> O + 0.25O <sub>2</sub> → NaOH  | NaOH                           | 1                               | 3.11             | 2083 <sup>a</sup><br>2604 <sup>b</sup>             | –300.1                             |
| K–O <sub>2</sub>  | K + O <sub>2</sub> → KO <sub>2</sub>                  | KO <sub>2</sub>                | 1                               | 2.48             | 935  | –239.4                             |

<sup>a</sup> Specific energy was estimated using all reactants Li, Na + 0.5H<sub>2</sub>O + 0.25O<sub>2</sub> and one electron. <sup>b</sup> Specific energy was estimated using Li, Na + 0.5H<sub>2</sub>O as reactants and one electron.

metal, forming KO<sub>2</sub> directly on the anode, thereby leading to the corrosion of the K metal. Ren *et al.* thoroughly characterised the side reaction on the anode.<sup>63</sup> Then, authors incorporated a polymeric potassium ion-selective membrane (Nafion-K<sup>+</sup>) to inhibit the side reactions of K metal using it as a separator. The authors suggested that excellent reversibility can be achieved by using an oxygen-corroded potassium anode. The K–O<sub>2</sub> battery using this Nafion-K<sup>+</sup> separator displayed 40 cycles of charge–discharge capability without any increase in charge overpotential (Fig. 4a). In contrast, it was observed that the discharge/charge potential gap increases significantly after the eighth cycle (Fig. 4b) in the K–O<sub>2</sub> cell without the K<sup>+</sup>-selective separator. With the Nafion-K<sup>+</sup> separator, the cell maintained a relatively stable potential gap (~0.3 V) for over 40 cycles, despite some resistance from the membrane. Additionally, it enhanced the coulombic efficiency to over 98% for most cycles.

Xiao *et al.* studied the long-term stability of superoxide KO<sub>2</sub> in K–O<sub>2</sub> batteries.<sup>64</sup> Their work explored the KO<sub>2</sub> electrochemistry using various instrumental techniques like chromatography method, SEM and NMR spectroscopy.<sup>63,64</sup> The reactivity and long-term stability of superoxide in K–O<sub>2</sub> batteries

are critical factors. To investigate the long-term stability of KO<sub>2</sub>, the authors conducted various experiments to analyse its electrochemistry and the formation of side products resulting from electrolyte decomposition in K–O<sub>2</sub> batteries. Their studies inferred that KF, HCOOK, and a small amount of CH<sub>3</sub>COOK and CH<sub>3</sub>OCH<sub>2</sub>COOK are the major side products of KPF<sub>6</sub> salt and 1,2-dimethoxyethane (DME) solvent. UV/Vis spectroscopy was utilised to study the deleterious effects of parasitic reactions on the coulombic efficiency of K–O<sub>2</sub> batteries. The reversible electrochemical process of KO<sub>2</sub> formation and decomposition at the cathode can prevent excessive side reactions in the electrode and electrolyte. However, the growth of KO<sub>2</sub> on the separator after dissolution can lead to a loss of electrons. It has been suggested that the “dead” KO<sub>2</sub> crystals lose their electrical connection with the carbon matrix, similar to the behaviour of Li<sub>2</sub>S in Li–S batteries. This loss of connection is believed to contribute to the irreversible portion of K–O<sub>2</sub> batteries. Enhancing the cathode material and its structure can potentially enhance the KO<sub>2</sub>/C contact and reduce the loss of KO<sub>2</sub> in the future. Also, if the resting period of K–O<sub>2</sub> batteries is increased, the over-potential increases and voltage

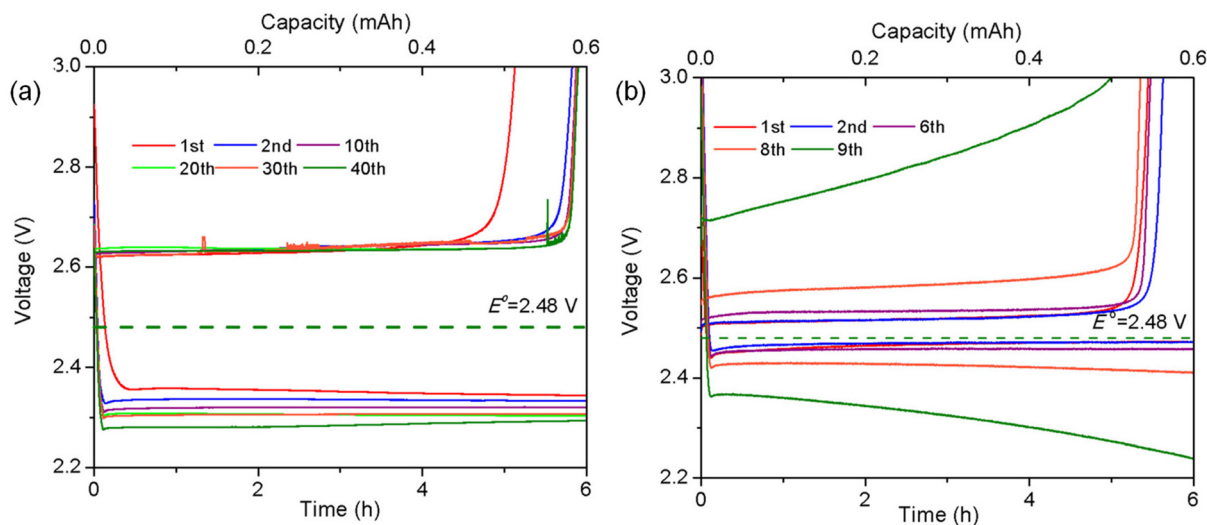


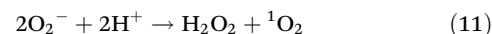
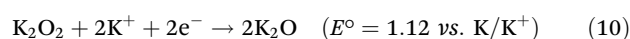
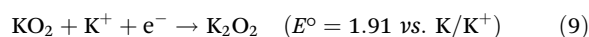
**Fig. 4** Galvanostatic discharge–charge voltage profiles of K–O<sub>2</sub> batteries (a) with and (b) without a Nafion-K<sup>+</sup> membrane for various cycles. Reproduced with permission from ref. 63. Copyright 2014 American Chemical Society.



fluctuations occur upon charging. This is due to the surface layer growth on the K-anode in the presence of oxygen. On further increasing the resting period, a stable layer of  $\text{KO}_2$  is formed on the anode surface, leading to the high coulombic efficiency of the battery.

The investigation conducted by the Yi-Chun Lu group delved into the electrode–electrolyte interface in metal–oxygen batteries,<sup>65</sup> particularly the K– $\text{O}_2$  chemistry, which is crucial in comprehending the reaction mechanisms. The study involved the investigation of the reaction mechanism of K– $\text{O}_2$  chemistry at the electrode–electrolyte interface by utilising Ambient Pressure X-ray Photoelectron Spectroscopy (APXPS) to analyse the ORR/OER in ionic liquid-based air batteries (Fig. 5a). Besides the commonly accepted one-electron mechanism, the findings showed additional reaction pathways in K– $\text{O}_2$  batteries. The study revealed that the formation and subsequent oxidation of potassium oxide ( $\text{K}_2\text{O}$ ) and potassium peroxide ( $\text{K}_2\text{O}_2$ ) can trigger irreversible cell reactions, potentially leading to capacity decay in K– $\text{O}_2$  batteries. The research also revealed that impurities such as  $\text{H}_2\text{O}$  and  $\text{CO}_2$  in the air can decrease the chemical reversibility of ORR and OER. These findings shed light on the underlying reasons for the irreversible cell chemistry in K– $\text{O}_2$  batteries. Additionally, the study suggests that APXPS analysis of ionic liquid-based air batteries is a valuable tool to investigate the chemistry of electrode–electrolyte interfaces in metal–air batteries.<sup>65</sup>

One of the significant findings of this work is the electrochemical reduction of  $\text{KO}_2$  to  $\text{K}_2\text{O}_2$  (Fig. 6a and eqn (9)) when discharging the cell to 1.91 V vs.  $\text{K}/\text{K}^+$ . Further lowering the cell discharge potential to 1.12 V vs.  $\text{K}/\text{K}^+$  leads to the formation of  $\text{K}_2\text{O}$  (eqn (10)). The presence of  $\text{K}_2\text{O}_2$  significantly reduces the coulombic and charging efficiencies of the K– $\text{O}_2$  battery, affecting its reversibility. Additionally, the formation of  $\text{K}_2\text{O}_2$  leads to a higher charging overpotential, requiring a higher voltage to charge the battery (Fig. 6b). The poor cell performance attributed to  $\text{K}_2\text{O}_2$  formation may be due to the generation of nucleophilic superoxide anions ( $\text{O}_2^-$ )<sup>66</sup> or singlet oxygen ( $^1\text{O}_2$ ).<sup>67</sup> The formed  $\text{O}_2^-$  during the oxidation of  $\text{K}_2\text{O}_2$  may lead to side reactions, such as attacking cell components or generating reactive singlet oxygen *via* eqn (10).<sup>67</sup> The authors suggested that a higher discharge cutoff voltage (above 2.2 V vs.  $\text{K}/\text{K}^+$ ) can prevent the formation of  $\text{K}_2\text{O}_2$  and improve battery reversibility.



In another key study, Küpper *et al.* investigated the effect of oxygen partial pressure on the discharge behavior and product of K– $\text{O}_2$  batteries by varying the pressure from 0.2 atm to 11

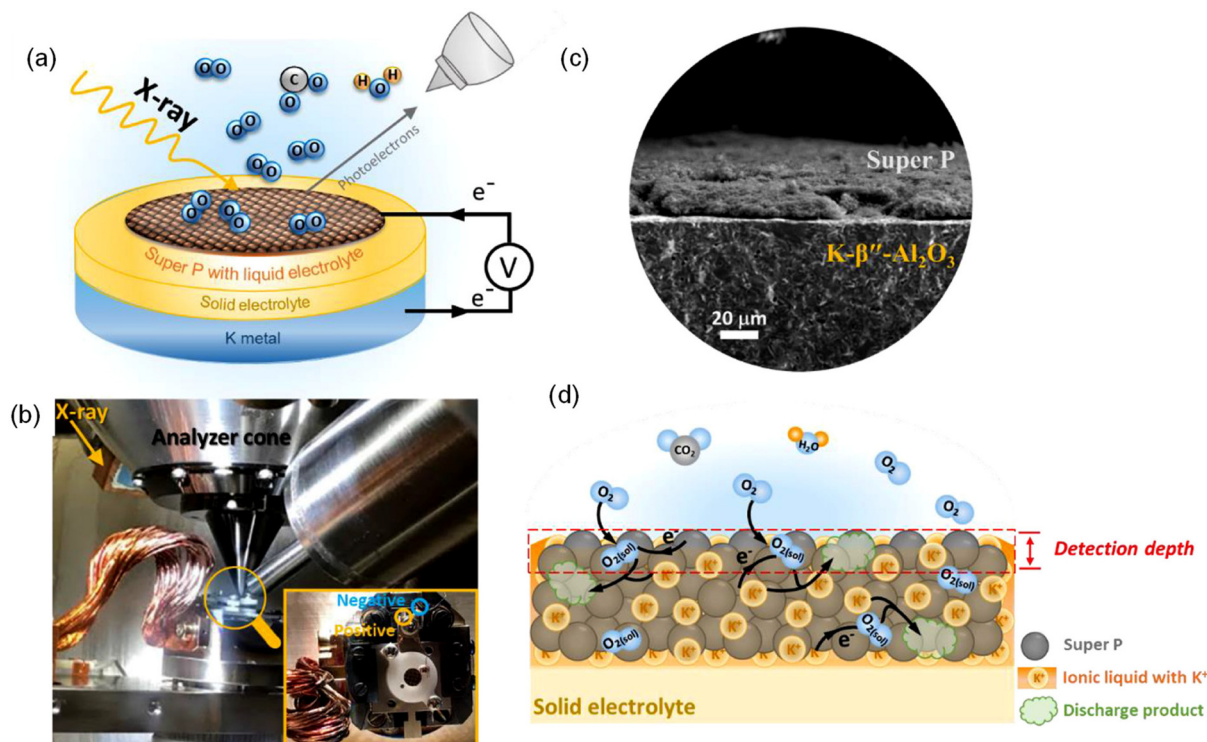


**Fig. 5** *In situ* APXPS measurements conducted on an ionic liquid-based porous K– $\text{O}_2$  battery. (a) The K– $\text{O}_2$  cell, comprising a K metal as the anode, K- $\beta''$ - $\text{Al}_2\text{O}_3$  solid electrolyte, and Super P carbon as the cathode with an ionic liquid electrolyte. (b) Image of the K– $\text{O}_2$  battery during APXPS analysis and (c) SEM cross-section of the carbon cathode and solid electrolyte. (d) Schematic of the APXPS sample detection depth, represented by the red dotted area. Reproduced with permission from ref. 65. Copyright 2021 Elsevier.



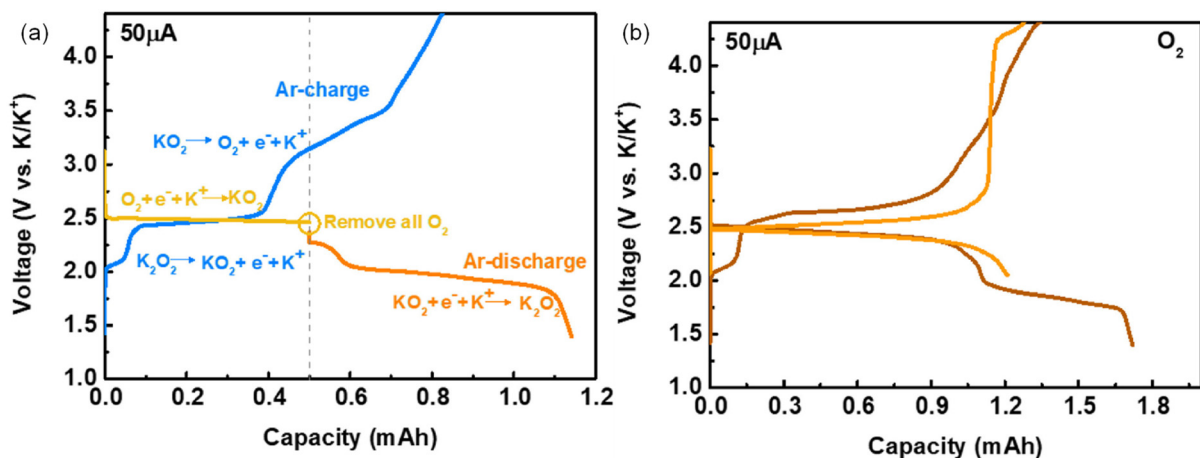


**Fig. 6** Galvanostatic charge–discharge profile of a K–O<sub>2</sub> cell showing the conversion of KO<sub>2</sub> to K<sub>2</sub>O<sub>2</sub> and its impact on the reversibility of the cell. (a) The cell was discharged up to 0.5 mAh in pure oxygen and then oxygen was replaced with argon, with continuous discharge followed by charging the cell under argon gas. (b) Galvanostatic charge–discharge at different cut-off capacities under an oxygen atmosphere. Reproduced with permission from ref. 65. Copyright 2021 Elsevier.

atm.<sup>68</sup> At low pressures (0.2–2 atm), representative of dry ambient conditions, the cells exhibited poor discharge performance and frequent failure due to severe oxygen transport limitations. These limitations led to incomplete cathode utilization, resulting in reduced discharge capacity and rate capability. Furthermore, oxygen depletion triggered parasitic reactions with the DMSO electrolyte, forming byproducts such as K<sub>2</sub>SO<sub>4</sub> and K<sub>2</sub>CO<sub>3</sub>. The discharge profiles under low-to-intermediate pressures showed multistage behavior, indicative of localized oxygen starvation. In contrast, high oxygen pressures (6–11 atm) significantly improved battery performance. A reduction in discharge overpotential by up to 150 mV was observed, along with a 13-fold increase in capacity at a high current density (1.0 mA cm<sup>-2</sup>) when increasing oxygen partial pressure from 0.2 to 11 atm. Elevated oxygen pressure prevented oxygen depletion, suppressed side reactions, and promoted uniform KO<sub>2</sub> deposition across the cathode. Overall, pressurizing K–O<sub>2</sub> batteries with pure oxygen (≥6 atm) effectively mitigates oxygen transport limitations and electrolyte degradation, thereby enhancing energy efficiency, rate capability, and cycling stability. This strategy offers a promising pathway toward realizing high-capacity, high-rate K–O<sub>2</sub> batteries for practical applications.

Liu *et al.* recently employed *in situ* Raman spectroscopy to gain deeper insights into the electrochemistry of K–O<sub>2</sub> batteries, focusing specifically on the oxygen-related redox processes.<sup>69</sup> For this study, the authors used a model system consisting of an Au electrode in a DMSO-based electrolyte. Their findings revealed that the key discharge products are KO<sub>2</sub> and K<sub>2</sub>O<sub>2</sub>, with superoxide (O<sub>2</sub><sup>-</sup>) identified as a critical intermediate whose formation is potential-dependent. At higher discharge potentials (>1.6 V vs. K/K<sup>+</sup>), molecular oxygen is first reduced to an O<sub>2</sub><sup>-\*</sup> radical anion, which desorbs from the Au electrode surface and enters the solution phase (Fig. 7a & b). There, it reacts with K<sup>+</sup> ions to form KO<sub>2</sub> *via* a solution-

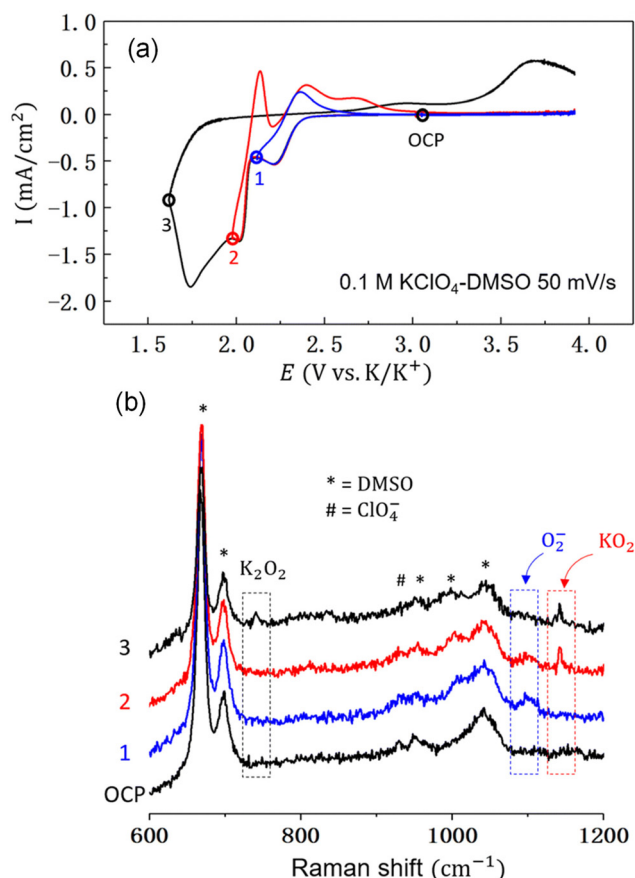


**Fig. 7** (a) CV recorded in O<sub>2</sub>-saturated 0.1 M KClO<sub>4</sub> in DMSO electrolyte. (b) Surface-enhanced Raman spectra of the Au electrode at different cut-off potentials and open-circuit potential (OCP). The blue curve corresponds to a cut-off potential of 2.12 V (1), the red to 1.98 V (2), and the black to 1.60 V vs. K/K<sup>+</sup> (3). Reproduced with permission from ref. 69. Copyright 2024 The Royal Society of Chemistry.



mediated mechanism. In contrast, at lower potentials, oxygen is directly reduced on the Au electrode surface to form an adsorbed  $\text{KO}_2^*$  intermediate, which can be further reduced to  $\text{K}_2\text{O}_2^*$  upon deep discharge ( $<1.6$  V vs.  $\text{K}/\text{K}^+$ ) (Fig. 7a & b). These observations suggest that  $\text{K}_2\text{O}_2$  is predominantly formed under high discharge overpotentials, and that  $\text{KO}_2$  does not undergo a disproportionation reaction during cycling. This study provides important mechanistic insights into the potential-dependent product distribution and electrochemical pathways in  $\text{K}-\text{O}_2$  batteries.

### 3. Literature review on $\text{K}-\text{O}_2$ batteries

This section provides a concise overview of the development of  $\text{K}-\text{O}_2$  batteries, including the electrolyte, air cathode, and anode. Each component of the cell is crucial in determining the life cycle, energy, and efficiency. The electrolyte facilitates ion transport and affects reaction kinetics, making its composition and stability essential for long-term cycling. The air cathode serves as the site for ORR/OER, influencing energy efficiency and discharge capacity. The anode, typically composed of potassium metal or its alternatives, significantly impacts battery lifespan and safety. An understanding of the design and optimization of these components is essential for improving  $\text{K}-\text{O}_2$  battery performance and addressing current challenges.

#### 3.1 Electrolytes for the $\text{K}-\text{O}_2$ battery

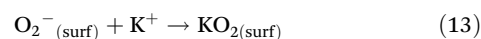
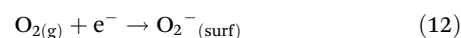
As is the case with all energy storage devices, the efficient movement of  $\text{K}^+$  ions between the electrodes is crucial in  $\text{K}-\text{O}_2$  batteries, and the choice of electrolyte is crucial as it can significantly affect the stability and performance of the battery, including rate performance, cycling stability and coulombic efficiency.<sup>70</sup> The ionic transport properties,  $\text{K}^+$  ion solvation properties and electrolytes' electrochemical stability greatly affect the batteries' performance. An ideal electrolyte should have high ionic conductivity, low desolvation energy and a large electrochemical stability window. Typically,  $\text{K}^+$  ions have weaker interactions (solvation shells) with solvent molecules compared to  $\text{Li}^+$  and  $\text{Na}^+$  ions due to the larger size, lower charge density and smaller Stokes radii of  $\text{K}^+$  ions, thereby enabling rapid ionic transport and higher ionic conductivity.<sup>71</sup> Also,  $\text{K}^+$  exhibited lower desolvation energy in most of the organic solvents compared to  $\text{Li}^+$  and  $\text{Na}^+$  ions, which also allows fast migration of  $\text{K}^+$  ions (Table 3).<sup>70</sup>

In metal- $\text{O}_2$  batteries, it has been found that the electrolyte affects the electrochemical performance of the air cathode, especially related to the discharge process. The discharge process can proceed *via* surface-mediated route or solution-mediated route as shown in eqn (12)–(16).<sup>73–75</sup> These cathodic processes involve three phases: solid–liquid–gas, and it is the electrolyte that determines whether the reaction is solution-mediated or surface-mediated.

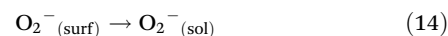
**Table 3** Desolvation energies associated with  $\text{Li}^+$ ,  $\text{Na}^+$  and  $\text{K}^+$  ions in common organic solvents<sup>70,72</sup>

| Solvent                        | Desolvation energy ( $\text{kJ mol}^{-1}$ ) |       |       |
|--------------------------------|---|-------|-------|
|                                | Li  | Na    | K     |
| Propylene carbonate (PC)       | 215.8                                       | 158.2 | 119.2 |
| Ethylene carbonate (EC)        | 208.9                                       | 152.8 | 114.6 |
| Diethyl carbonate (DEC)        | 205.6                                       | 147.9 | 105.1 |
| Ethyl methyl carbonate (EMC)   | 199.1                                       | 143.1 | 101.6 |
| Fluoroethylene carbonate (FEC) | 188.8                                       | 136.2 | 100.5 |
| Vinylene carbonate (VC)        | 191.4                                       | 138.3 | 102.2 |
| Butylene carbonate (BC)        | 219.5                                       | 161.4 | 121.9 |
| Trimethyl phosphate (TMP)      | 249.1                                       | 181.2 | 135.4 |
| Dimethyl formamide (DMF)       | 230.1                                       | 165.5 | 122.8 |
| Dimethyl sulfoxide (DMSO)      | 232.9                                       | 167.8 | 125   |
| N-Methyl-2-pyrrolidone (NMP)   | 243.6                                       | 175.5 | 131   |

Surface-mediated route:



Solution-mediated route:



In general, ester- and ether-based electrolytes have been used in potassium batteries.<sup>76</sup> However, it was an ether-based electrolyte which was employed in  $\text{K}-\text{O}_2$  battery as ethers have generally been considered to be relatively safe with K metal (ethers have less reactive oxygen atoms as they are bonded to two carbon atoms).<sup>77</sup> Moreover, due to the low desolvation process and fast oxygen diffusion kinetics, ether-based electrolytes also provide moderate discharge capacities at moderate current densities.<sup>14,73</sup> Lastly, ether-based solvent promotes the growth of  $\text{KO}_2$  *via* a solution-mediated route.<sup>78</sup> In the first study on  $\text{K}-\text{O}_2$  batteries, Ren *et al.* used 0.5 M  $\text{KPF}_6$  dissolved in either DME or a butyl diglyme/diglyme mixture (v/v 2 : 5) as the electrolyte.<sup>25</sup> This work validated the concept and reversibility of  $\text{K}-\text{O}_2$  batteries; however, the rechargeability of the cell in this electrolyte was poor, as the cell capacity dropped by nearly half in the second cycle (Fig. 8). This degradation was primarily attributed to the diffusion of side products to the metal electrode, forming an insulating layer. Consequently, the charging voltage increased in subsequent cycles compared to the first cycle.

Wang *et al.* investigated the reversibility and energy efficiency of  $\text{K}-\text{O}_2$  batteries in dimethyl sulfoxide (DMSO) and compared it with those from a diethylene glycol dimethyl ether (diglyme)-based electrolyte (0.5 M  $\text{KPF}_6$  in both solvents).<sup>79</sup> They observed that the cell tested in DMSO exhibited higher reversibility and energy efficiency than the one with diglyme. This improvement was attributed to the stronger electron-donating ability of DMSO ( $29.8 \text{ kcal mol}^{-1}$  donor



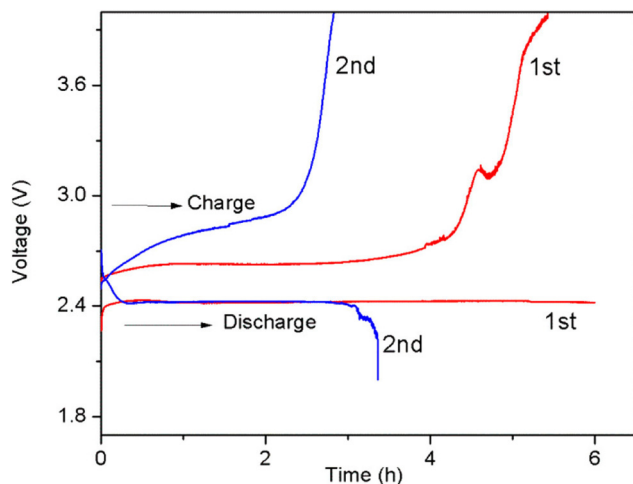


**Fig. 8** Initial two continuous discharge-charge cycles of the battery at a current density of  $0.16 \text{ mA cm}^{-2}$  in a  $0.5 \text{ M KPF}_6$  electrolyte solution composed of butyl diglyme and diglyme (2:5 v/v ratio). Reproduced with permission from ref. 25. Copyright 2013 American Chemical Society.

number)<sup>80</sup> than diglyme ( $\sim 24 \text{ kcal mol}^{-1}$  donor number),<sup>81</sup> which stabilizes  $\text{KO}_2$ , enhancing electrode kinetics and chemical/electrochemical reversibility. The authors emphasized that an ideal solvent for  $\text{K-O}_2$  batteries should strongly stabilize superoxide to ensure fast reaction kinetics and high reversibility. Furthermore, they noted that the lower capacity results from dendritic  $\text{KO}_2$  covering the electrode. This issue can be mitigated using a solvent with higher  $\text{O}_2$  solubility and lower viscosity, which improves  $\text{O}_2$  diffusion, reduces concentration gradients, and promotes cubic  $\text{KO}_2$  formation. Sankarasubramanian *et al.* further proposed DMSO as an effective solvent for the selective production of  $\text{KO}_2$ , enhancing the rechargeability of  $\text{K-O}_2$  batteries.<sup>82</sup> They also observed that the first electron transfer rate constant associated with ORR is four orders of magnitude higher in DMSO compared to ether-based electrolytes, contributing to a significantly improved rate capability. Though DMSO solvent-based electrolytes showed improved reversibility and energy efficiency, surface-

confined  $\text{KO}_2$  growth and low discharge capacities remain challenges owing to the high desolvation energy barrier of  $\text{K}^+$  ions and limited oxygen diffusion. Recent studies highlight the importance of solvent properties and electrolyte structure in improving  $\text{K-O}_2$  battery cathode performance.<sup>78</sup> However, an optimized electrolyte design is still needed to enhance capacity and efficiency. The use of a co-solvation strategy that involves DME and DMSO has been demonstrated to decrease the overpotential necessary for cathodic reactions and improve the cathode discharge capacity. The solution-mediated growth of  $\text{KO}_2$  and its stripping from the cathode surface during cycling were facilitated by the improved solvation structure, which led to a significant improvement in coulombic efficiency for the cathode.<sup>73</sup> A summary of electrolytes utilized in  $\text{K-O}_2$  batteries is provided in Table 4<sup>14</sup> which highlights the current density, capacity, and charge/discharge potential gap across different studies, reflecting variations in electrolyte composition and battery configuration.

A study has also been performed to investigate the kinetics of ORR in  $\text{KO}_2$  batteries by using rotating ring-disk electrode (RDE) techniques and differential electrochemical mass spectrometry with DMSO-based electrolytes.<sup>83</sup> The presence of  $\text{K}^+$  ions in DMSO was credited to the formation of sparingly soluble  $\text{KO}_2$  and insoluble  $\text{K}_2\text{O}_2$  with two reduction processes. The choice of electrode material has been shown to exert a considerable influence on the rate and efficiency of oxygen reduction to superoxide. Specifically, glassy carbon electrodes facilitate this reaction much more readily than gold electrodes, a result that calls into question the conventional assumption of a straightforward outer-sphere mechanism and highlights the importance of electrode surface properties in these processes. The importance of ion pairing between  $\text{K}^+$  ions and superoxide, with  $\text{KClO}_4$  stabilizing superoxide and shifting half-wave potentials to more favorable values compared to electrolytes containing tetrabutylammonium cation. This has been shown to promote significant ion-pairing between superoxide and  $\text{K}^+$  ions, resulting in a shift of the half-wave potential toward more positive values. The ion-pairing constant was determined to be  $K_{\text{ion}} = 7.25 \times 10^2 \text{ mol L}^{-1}$ . This stabilization effect, quantified by an equilibrium constant for superoxide- $\text{K}^+$  ion pairing, indicates that the influence of potassium

**Table 4** List of electrolytes used in  $\text{K-O}_2$  batteries with capacities and potential gaps with cycles

| Electrolyte   | Current density                   | Capacity                               | <sup>b</sup> Potential gap (V)/cycle | Ref. |
|---|-----------------------------------|--|--------------------------------------|------|
| 0.5 M $\text{KPF}_6$ in butyl diglyme/diglyme                                     | $0.16 \text{ mA cm}^{-2}$         | $0.96 \text{ mAh cm}^{-2}$             | 0.25/1; 0.45/2                       | 25   |
| 0.5 M $\text{KPF}_6$ in DME   | $0.065 \text{ mA cm}^{-2}$        | $0.39 \text{ mAh cm}^{-2}$             | 0.3/1; 0.35/40                       | 63   |
| 0.5 M $\text{KPF}_6$ in DME   | $20 \text{ mA g}^{-1}$            | 0.3 mAh                                | 0.25/1; 0.55/8                       | 84   |
| 0.5 M $\text{KPF}_6$ in DME   | $1 \text{ A g}^{-1}$ <sup>a</sup> | $1000 \text{ mAh g}^{-1}$ <sup>a</sup> | 0.1/1; 0.4/200                       | 75   |
| 1 M KTFSI in DME  | 0.25 mA                           | 0.25 mAh                               |                                      |      |
| 0.5 M $\text{KPF}_6$ in diglyme   | $0.04 \text{ mA cm}^{-2}$         | $0.24 \text{ mAh cm}^{-2}$             | 0.4/1; 0.4/60                        | 85   |
| 0.5 M $\text{KPF}_6$ in diglyme   | $0.05 \text{ mA cm}^{-2}$         | $0.25 \text{ mAh cm}^{-2}$             | 0.05/1; 0.4/70                       | 86   |
| 0.5 M $\text{KPF}_6$ in DMSO (cathode) and 0.5 M $\text{KPF}_6$ in DEGDME (anode) | $0.885 \text{ mA cm}^{-2}$        | $0.221 \text{ mAh cm}^{-2}$            | 0.3/1; 0.55/200                      | 79   |
| 0.5 M $\text{KPF}_6$ in DMSO (cathode only)                                       | $2 \text{ mA cm}^{-2}$            | $0.25 \text{ mAh cm}^{-2}$             | 0.53/1; 0.63/2000                    | 87   |
| 0.5 M KTFSI in DME/DMSO   | $0.25 \text{ mA cm}^{-2}$         | $4.97 \text{ mAh cm}^{-2}$             | 0.04/1; $\sim 0.04/180$              | 73   |

<sup>a</sup> Estimated based on rGO weight. <sup>b</sup> Potential gap in the first cycle and then gap in the last cycle.



cannot be fully explained by conventional Pearson acid–base concepts. Additionally, the presence of water in K–O<sub>2</sub> systems exhibits a unique effect: isotopic labeling experiments demonstrate that water actually suppresses the formation of K<sub>2</sub>O<sub>2</sub>, contrary to its role in lithium-based electrolytes. Intriguingly, during the oxidation of species deposited on the electrode, an unexpected consumption of oxygen is observed, which has been linked to increased CO<sub>2</sub> evolution, further complicating the picture of how oxygen and potassium ions interact in these advanced battery systems. However, the study suggests that in general the K–O<sub>2</sub> battery system is a very interesting system as it exhibits well-defined and stable electrochemical behaviour which makes it an attractive candidate for future battery research.

Qin *et al.* introduced a “solvent-in-anion” strategy to enhance the reversibility of KO<sub>2</sub>/K<sub>2</sub>O<sub>2</sub> redox reactions in K–O<sub>2</sub> batteries.<sup>88</sup> By incorporating a high-donicity anion additive into a moderately solvating ether-based electrolyte, the authors aimed to modulate electron donicity and stabilize KO<sub>2</sub>, thereby enabling catalyst-free, solution-mediated K<sub>2</sub>O<sub>2</sub> decomposition. Specifically, the anion additive, (3-methoxypropyl)((trifluoromethyl)sulfonyl)amide (MPSA<sup>−</sup>), was added to a 0.5 M KPF<sub>6</sub>/DME electrolyte, achieving compatibility across the anode–electrolyte–cathode interfaces. This approach established a solution-mediated KO<sub>2</sub>/K<sub>2</sub>O<sub>2</sub> interconversion pathway with a low overpotential of 216 mV. The K/KO<sub>2</sub> full cell delivered a specific capacity of 292 mAh g<sup>−1</sup> (based on KO<sub>2</sub> mass), maintained a round-trip efficiency of 84.4%, and operated stably over 120 cycles at 85.4% depth of discharge without an electrocatalyst. Importantly, the cell functioned as a closed, O<sub>2</sub>-free system, mitigating gas-related degradation and electrolyte evaporation. Overall, this work demonstrates that high-donicity anions can enable reversible two-electron KO<sub>2</sub>/K<sub>2</sub>O<sub>2</sub> chemistry without reliance on solid catalysts, offering improved energy efficiency and redox reversibility. However, the study did not investigate the compatibility between high-donicity anions and K metal, which can lead to uncontrolled side reactions at the anode–electrolyte interface and limited full-cell cycle life. Additionally, no strategies were proposed to mitigate K anode corrosion or passivation critical challenges for practical application.<sup>31,78</sup>

In addition to liquid electrolytes, solid-state electrolytes have also been tested for K–O<sub>2</sub> batteries to enhance the safety of the cell as K metal is highly reactive. To address this, Shao *et al.* developed a barium-doped K<sub>3</sub>SbSe<sub>4</sub> solid-state electrolyte.<sup>89</sup> By substituting Ba<sup>2+</sup> for K<sup>+</sup>, the authors introduced K vacancies, expanded the lattice, and induced a phase transition from trigonal to cubic symmetry. This structural transformation enabled enhanced K<sup>+</sup> ion mobility, resulting in a high ionic conductivity of 0.1 mS cm<sup>−1</sup> at 40 °C for K<sub>2.2</sub>Ba<sub>0.4</sub>SbSe<sub>4</sub>, over two orders of magnitude higher than the undoped material. The cubic framework facilitated three-dimensional K<sup>+</sup> ion diffusion pathways, significantly reducing interfacial resistance. Using this optimized electrolyte, the authors demonstrated a two-compartment K–O<sub>2</sub> battery separated by a solid-state electrolyte that operated for 100 cycles

without notable degradation, retaining a maximum capacity of ~0.055 mAh with an average coulombic efficiency of 94%. Additionally, the solid-state design effectively prevented oxygen crossover and allowed for the flexible use of different anolytes and catholytes, improving safety and compatibility. Additionally, a water-mediated, super-correlated proton-assisted transport mechanism was employed to support the feasibility of solid-state K–O<sub>2</sub> batteries, demonstrating stable cycling and enhanced energy efficiency, thereby advancing the development of safer and higher-performing K–O<sub>2</sub> systems.<sup>90</sup> However, the study does not address the long-term chemical and electrochemical stability of water within the solid electrolyte matrix, which remains a critical concern for practical implementation.

The selection of a suitable electrolyte for K–O<sub>2</sub> batteries depends on multiple factors, including electrode materials, targeted performance metrics, and safety and stability requirements. Ongoing research focuses on developing and optimizing electrolyte compositions to enhance the overall performance and reliability of K–O<sub>2</sub> batteries.

### 3.2. Air cathode for the K–O<sub>2</sub> battery

An ideal air electrode in rechargeable metal–O<sub>2</sub> batteries should have a highly porous structure (2–50 nm pore size) to allow efficient oxygen and electrolyte diffusion, as microscopic pores (<2 nm) can block oxygen flow and limit catalytic activity.<sup>21</sup> It must also possess good electrical conductivity to facilitate smooth electron transfer. Additionally, bifunctional catalytic activity is essential, enabling the electrode to efficiently catalyze both charging (OER) and discharging (ORR) reactions. This improves energy efficiency, enhances cycle stability, and reduces energy losses due to high overpotentials. It would be worth saying that most of the research in K–O<sub>2</sub> batteries is focused on the development of electrolytes and understanding the reaction mechanisms of both K metal and air electrodes. Nonetheless, thanks to the electrochemistry of K–O<sub>2</sub> batteries, they do not require high-performance catalysts. This is evident from the fact that most air cathodes tested in K–O<sub>2</sub> batteries are made of carbon-based materials such as Super P carbon black, reduced graphene oxide (rGO), and carbon nanotubes. One such example is the utilization of rGO as a cathode by Xiao *et al.* to demonstrate high-capacity K–O<sub>2</sub> batteries.<sup>75</sup> A thin, porous rGO cathode has manifold advantages like high specific surface area and pore volume to facilitate oxygen transport and KO<sub>2</sub> deposition. High specific surface area and pore volume of a thin porous rGO cathode facilitate the KO<sub>2</sub> deposition and oxygen transport. Additionally, the high aspect ratio of rGO material provides a large accessible surface area for ORR without any restrictions for pore width. In an rGO-based K–O<sub>2</sub> battery, an overall capacity of more than 8400 mAh g<sup>−1</sup> is attained at a current density of 1000 mA g<sup>−1</sup> carbon (Fig. 9a). Furthermore, up to 200 cycles with charge and discharge cycles equivalent to more than 400 h were observed as presented in (Fig. 9b & c). By restricting the discharge depth to 1000 mAh g<sup>−1</sup>, the carbon and rGO electrode battery maintains stable discharge/charge capacities and coulombic efficiency



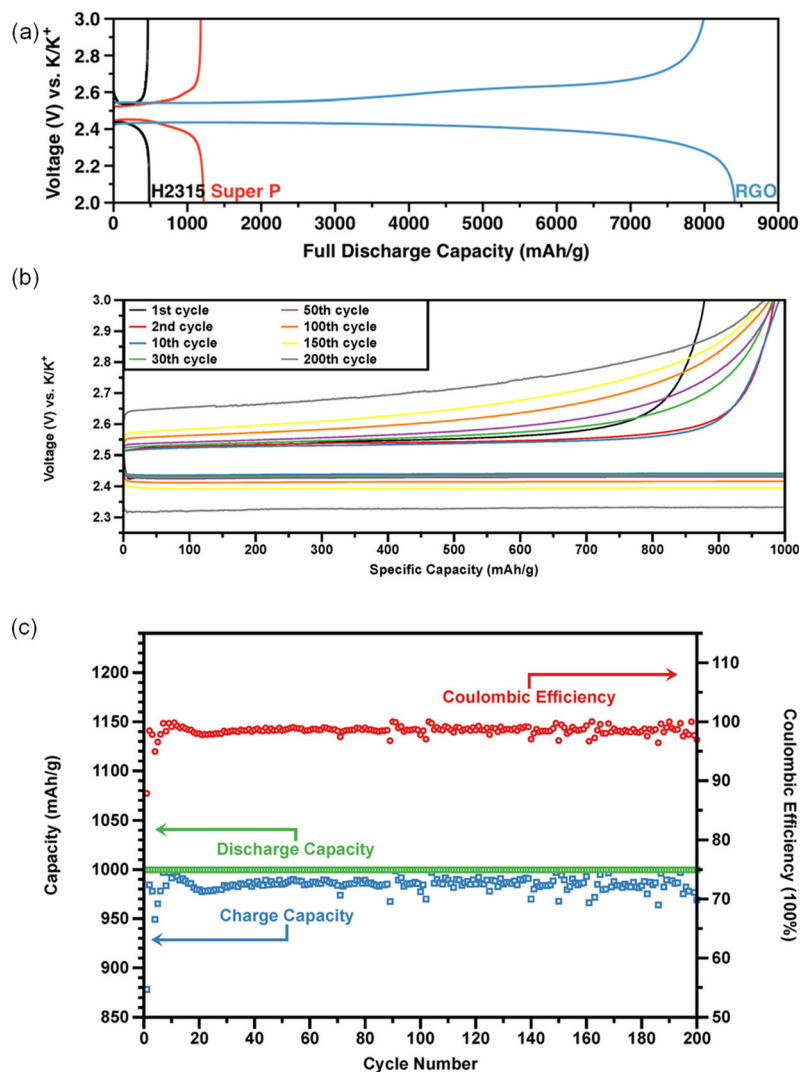


**Fig. 9** (a) Discharge capacities related to the first cycle of carbon fiber electrodes (H2315 Freudenberg FCCT SE & Co. KG), Super P and rGO electrodes; (b) GCD of rGO electrodes upon cycling, and (c) cycling stability of the rGO electrode at 1000 mA g<sup>-1</sup> current rate. Reproduced with permission from ref. 75. Copyright 2016 American Chemical Society.

(~98%) throughout the cycling test. The upsurge of overpotential with the cycle number is mainly due to the oxygen cross-over issue in the battery setup. The traversed oxygen is accountable for a thick layer of KO<sub>2</sub> and other by-products on the anode surface. It is fascinating that the rGO-based K-O<sub>2</sub> battery maintains its original high round-trip efficiency. It also shows a considerable enhancement in the cycle number. Besides carbon materials, Zhang *et al.* recently tested a mulberry-like Ag/AgCl@TiO<sub>2</sub>/V<sub>2</sub>O<sub>5-x</sub> composite as an air cathode for a long-life K-O<sub>2</sub> battery.<sup>91</sup> The K-O<sub>2</sub> battery exhibited 1392 mAh g<sup>-1</sup> discharge capacity with 80 times long cycle life.

Dou and colleagues introduced an innovative cathode design which is a hierarchical porous carbon nanotube sphere (CNTS) with macropores forming between CNTS and nanopores inside each CNTS for K-O<sub>2</sub> batteries, targeting enhanced cycling stability, round-trip efficiency and rate performance compared to traditional carbon-based cathodes.<sup>92</sup> This archi-

tecture enhances cyclic stability, round-trip efficiency, and rate performance compared to traditional carbon-based cathodes. Efficient oxygen diffusion and electrolyte access are promoted throughout the electrode, while the high surface area provides abundant active sites for electrochemical reactions. Comprehensive analyses including coulometry, FTIR, Raman spectroscopy, and XRD reveal a strong correlation between the carbon cathode's structure and the resulting KO<sub>2</sub> morphology, which significantly impacts K-O<sub>2</sub> battery performance. The hierarchical porosity ensures uniform distribution of discharge products and facilitates their decomposition during charging, reducing overpotential and improving energy efficiency. The robust structure accommodates volume changes and resists degradation, resulting in durable long-term operation. Notably, the CNTS cathode showed an average discharge voltage of 2.38 V, an average coulombic efficiency of 95.8% and over 40 cycles of stable cycling with minimal capacity fade.



Overall, this study highlights the advantages of tailored porous carbon architectures in advancing K-O<sub>2</sub> battery technology and demonstrates that hierarchical porous carbon nanotube spheres are highly promising for next-generation high-performance energy storage applications.

Furthermore, Singh *et al.* recently proposed a method to enhance cathode performance in K-O<sub>2</sub> batteries through thermal oxidation of carbon paper, commonly used as the air electrode substrate, over varying durations (4 to 24 hours).<sup>93</sup> This treatment yielded a hierarchical porous carbon structure enriched with oxygen-containing surface functional groups. The resulting micro-, meso-, and macro-porosity improved O<sub>2</sub>/K<sup>+</sup> transport and increased access to active sites, leading to a significant enhancement in discharge capacity from 3.5 mAh cm<sup>-2</sup> (untreated) to 5 mAh cm<sup>-2</sup> (Fig. 10a-d). The higher

surface area exhibited high charge storage capacity at all current, whereas the formation of surface O-C=O groups facilitated KO<sub>2</sub> nucleation and improved the carbon/electrolyte interfacial stability, thereby reducing the discharge potential by 0.03 V (Fig. 10e and f). This work demonstrates that synergistically engineering cathode porosity and surface chemistry effectively addresses key limitations in oxygen reactivity and ion diffusion, enabling higher capacity and energy-efficient discharge performance. However, the study primarily focuses on discharge behaviour. Critical aspects related to rechargeability such as the evolution of discharge overpotential during cycling, the long-term stability of oxygen-containing groups, and the structural integrity of the porous network under repeated KO<sub>2</sub> formation/decomposition, remain unexplored.



**Fig. 10** Discharge curves of K-O<sub>2</sub> cells with the cathode (a) untreated, and treated for (b) 4 h, (c) 12 h and (d) 24 h at different current densities (0.1 mA cm<sup>-2</sup> in pink, 0.5 mA cm<sup>-2</sup> in blue and 1 mA cm<sup>-2</sup> in green). The dashed black line in the discharge profiles presents the open circuit voltage, *i.e.*, 2.18 V. Relationship of (e) areal discharge capacity with the surface area and (f) discharge overpotential with the O/C ratio. The colour coding is the same as in the discharge profiles. Reproduced with permission from ref. 93. Copyright 2024 by the authors. Licensee MDPI, Basel, Switzerland.



Qiao *et al.* demonstrated that integrating  $\text{KO}_2$  into a hybrid catalytic system comprising ruthenium dioxide ( $\text{RuO}_2$ ) nanoparticles anchored on an rGO framework enables a non- $\text{O}_2$ -evolving, reversible  $\text{KO}_2/\text{K}_2\text{O}_2$  interconversion (Fig. 11a).<sup>66</sup> Their investigation identifies  $\text{O}_2^-$  anion generation as the primary cause of irreversible  $\text{O}_2$  release and electrolyte degradation. To address this, they engineered a novel K-deficient  $\text{K}_{1-x}\text{O}_2\text{-Ru}$  interfacial phase during charging, which effectively suppresses  $\text{O}_2^-$  anion formation and stabilizes the electrode-electrolyte interface. Transmission electron microscopy (TEM) and XRD analyses confirm the homogeneity of the composite, showing  $\text{KO}_2$  nanoparticles (10–15 nm) well-embedded within the  $\text{RuO}_2\text{@rGO}$  matrix (Fig. 11b). Electrochemical testing

reveals that the  $\text{RuO}_2$ -free  $\text{KO}_2\text{-rGO}$  cathode (gray curve, Fig. 11c) undergoes a sharp potential rise during charging, surpassing the theoretical OER potentials of both  $\text{K}_2\text{O}_2$  (2.2 V) and  $\text{KO}_2$  (2.48 V), indicating irreversible  $\text{O}_2$  evolution. In contrast, the  $\text{KO}_2\text{-RuO}_2\text{@rGO}$  cathode (blue curve, Fig. 11c) exhibits a pronounced and stable discharge plateau at an average voltage of 1.88 V vs.  $\text{K/K}^+$ , with a minimal overpotential of 0.06 V relative to the theoretical value. This configuration achieves a high specific capacity of  $355.6 \text{ mAh g}^{-1}$ , corresponding to 94.3% utilization of the theoretical capacity. The optimized half-cell configuration demonstrates exceptional cycling stability, with a minimal average overpotential of 0.2 V and a capacity of  $300 \text{ mAh g}^{-1}$  (relative to preloaded  $\text{KO}_2$  mass) sus-

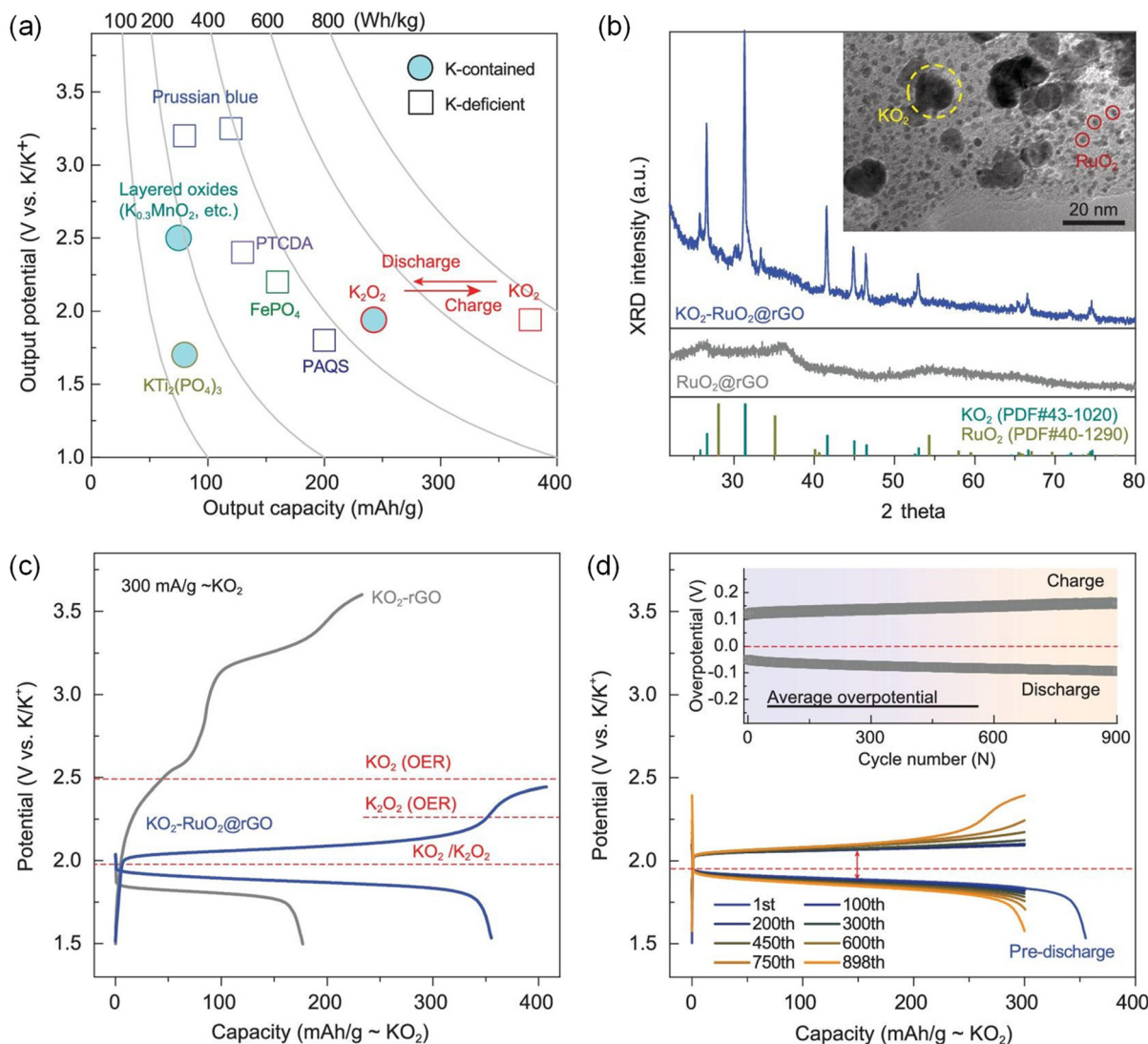


**Fig. 11** Electrochemical and structural analysis of  $\text{KO}_2$ -based cathodes in potassium-ion batteries. (a) Theoretical comparison of output potential, capacity, and energy density for  $\text{KO}_2$  cathodes contrasted with K-ion cathode materials. (b) Material characterization: XRD and TEM of the  $\text{KO}_2\text{-RuO}_2\text{@rGO}$  composite, compared with  $\text{KO}_2\text{-rGO}$ . (c) Initial cycle profiles: GCD plot of  $\text{KO}_2\text{-rGO}$  (gray) and  $\text{KO}_2\text{-RuO}_2\text{@rGO}$  (blue) cathodes during the first cycle at  $300 \text{ mA g}^{-1}$ . (d) Half-cell performance: charge–discharge plot of  $\text{KO}_2\text{-RuO}_2\text{@rGO}$  with a K metal anode, an average voltage overpotential of 0.2 V (inset) relative to 1.94 V, and current density  $300 \text{ mA g}^{-1}$ . Reproduced with permission from ref. 66. Copyright 2020, The Author(s) 2020. Published by Oxford University Press on behalf of China Science Publishing & Media Ltd.



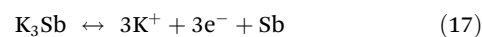
tained over 900 cycles (Fig. 11d). Furthermore, full-cell assemblies incorporating a modified electrolyte and a limited-excess potassium-metal anode achieve outstanding cyclability, rivaling leading potassium-ion battery technologies. This work represents a significant advancement in the development of high-capacity, long-life potassium-metal batteries by overcoming the key challenge of irreversible oxygen evolution. However, issues like electrolyte stability towards the reactive  $O_2^-$  anion, cost of materials, electrocatalysts and K metal issues remain a challenge.

### 3.3. Anode in the K-O<sub>2</sub> battery

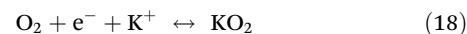
The role of K metal as an anode significantly affects the performance of K-O<sub>2</sub> batteries, such as energy efficiency and cycling stability. It has been realised that the reactivity of K metal challenges battery life and safety.<sup>94</sup> Dendritic growth due to repeated cycling, oxygen crossover and electrolyte degradation are the critical issues associated with K metal.<sup>63,78,95</sup> These challenges have led to research on improving and stabilising the anode. To design and develop a high-performance anode, one must comprehend the underlying efficiency parameters, like interfacial chemistry, electrolytic functions, ion diffusion in solid electrodes and correlation between them in K-O<sub>2</sub> batteries.<sup>42</sup> Hence, the main challenges undermining the performance of K-O<sub>2</sub> batteries must be appropriately addressed while designing these batteries. Surface coatings can mitigate any undesirable surface reactions that may persist due to nanostructures with a high surface area. McCulloch *et al.* showed a successful approach for modifying the anode material, resulting in a high-capacity K-O<sub>2</sub> battery.<sup>84</sup> An antimony-based electrode exhibits an average discharge voltage of 1.8 V (Fig. 12a) and a reversible storage capacity of 650 mAh g<sup>-1</sup> (98% of the theoretical capacity of 660 mAh g<sup>-1</sup>) corresponding to the formation of a cubic K<sub>3</sub>Sb alloy. Antimony has

been suggested as a promising anode material for various metal-ion batteries owing to its high theoretical capacity. McCulloch *et al.* employed a K-Sb alloy anode to demonstrate high-capacity performance in K-O<sub>2</sub> batteries, with reversible cycling capability (Fig. 12b). The K<sub>3</sub>Sb-O<sub>2</sub> cell exhibited low overpotential and a high operating voltage. However, a major limitation arises from the substantial ~407% volume expansion of antimony upon alloying with K, leading to continuous capacity fading. To mitigate this issue, researchers have encapsulated Sb nanoparticles within a carbon matrix to buffer the volume changes. The key advantage of the carbon matrix is its ability to provide an efficient conduction pathway.<sup>34</sup> Hence, the high capacity of Sb/C nanocomposites is attributed to the formation of K<sub>3</sub>Sb antimonide. The anodic and cathodic reactions of the K<sub>3</sub>Sb-C battery during discharge can be expressed using eqn (17) and (18):

At the anode



At the cathode:



The process of charging and discharging results in volume expansion of the electrode, which can cause pulverisation, creating dead areas that are electrically isolated from conductive agents, ultimately leading to capacity fading. To mitigate this issue, a soft and conductive matrix can buffer the volume changes during charging and discharging. In general, to ensure effective interfacial contact, the solvent in the electrolyte of K-O<sub>2</sub> batteries tends to undergo reduction readily on the electrode surface. This possibility might be correlated to the lower redox potential of K<sup>+</sup>/K. The lower the initial coulombic efficiency at lower cut-off voltages, the higher the prob-

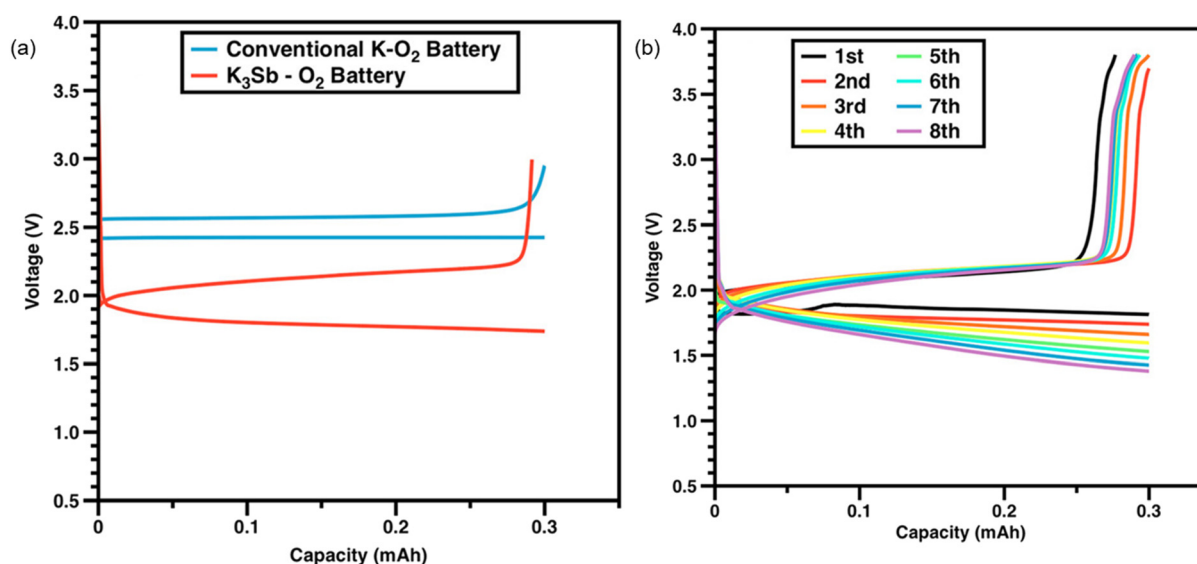


Fig. 12 (a) Galvanostatic discharge/charge profiles of a conventional K-O<sub>2</sub> battery and a K<sub>3</sub>Sb-O<sub>2</sub> battery. (b) Cycling performance of the K<sub>3</sub>Sb-O<sub>2</sub> battery. Reproduced with permission from ref. 84. Copyright 2015 American Chemical Society.



ability of occurrence of side reactions at those voltages. These side reactions are detrimental to battery performance and consume more electrolytes, causing the drying of batteries. Consequently, there is a sharp increase in polarization, thereby degrading the electrode capacity.<sup>96</sup> Dendrite growth is another major problem severely affecting the battery performance as well as their safe usage. Yu *et al.* suggested a solution by developing a liquid alloy anode for K–O<sub>2</sub> battery.<sup>86</sup> The mechanistic studies for assessing the parameters controlling the capacity and rate performance of metal–O<sub>2</sub> batteries based on superoxide were performed by Xiao *et al.* The possibility of two feasible processes for the growth of KO<sub>2</sub> was proposed. In the first process, K<sup>+</sup> ions from the electrolyte react with reduced oxygen on the cathode surface to form KO<sub>2</sub> crystals. In the second process, electrons transfer through the KO<sub>2</sub> crystal surface and react with oxygen and K<sup>+</sup> ions. The process of formation and distribution of KO<sub>2</sub> is almost like the formation of NaO<sub>2</sub> and Li<sub>2</sub>O<sub>2</sub> in Na–O<sub>2</sub> and Li–O<sub>2</sub> batteries, respectively, but the disproportionation step in the Li–O<sub>2</sub> battery is absent for K–O<sub>2</sub> batteries.<sup>97,98</sup> According to the authors, optimizing the cathode materials will be crucial in enhancing the overall capacity and rate capability of K–O<sub>2</sub> batteries. The authors achieved a dendrite-free K–O<sub>2</sub> battery at room temperature using a liquid Na–K alloy, exhibiting a 2.45 V discharge plateau at 0.05 mA cm<sup>-2</sup>.<sup>86</sup> A robust and stable liquid–liquid interface was established between the liquid alloy anode and the liquid electrolyte, ensuring high battery performance. The authors also tested this alloy anode in Na–O<sub>2</sub> batteries but found that it was only compatible with K–O<sub>2</sub> systems. This was attributed to potassium's stronger reducibility and the formation of the thermodynamically favourable KO<sub>2</sub> over NaO<sub>2</sub> during discharge. The liquid alloy anode enabled a long battery lifespan of up to 620 hours and a low discharge–charge overpotential of 0.05 V. However, challenges such as oxygen crossover and ether–electrolyte instability remain, affecting overall battery performance. A biphenyl-K (BpK) liquid anode was also investigated as an anode in combination with a DMSO-mediated air cathode.<sup>99</sup> The proposed battery concept showed cycling stability up to 3000 cycles, with a higher average coulombic efficiency >99.84% at a relatively high current density of 4.0 mA cm<sup>-2</sup>. This superior performance could be attributed to the suppression of dendritic growth at the anode and minimizing unstable interface and crosstalk between anode, electrolyte and cathode, which includes addressing issues related to oxygen or KO<sub>2</sub> crossover and other chemical reactions between cathode and anode. In addition to these, potassiated graphite was also used as an anode in K–O<sub>2</sub> batteries, which showed reversibility up to 80 cycles with >90% energy efficiency at a depth of discharge of 25%.<sup>100</sup> In addition to these strategies, potassium graphite intercalation compounds were also investigated by Yu Lei and team to address the longstanding challenges associated with metal anodes in K–O<sub>2</sub> batteries, such as severe volume expansion, dendrite growth, and instability due to oxygen crossover.<sup>101</sup> Their strategy was to replace the conventional K metal anode with graphite intercalation compound (GIC) anode, making both cathode

and anode carbon-based materials. Through this novel design, a robust solid electrolyte interphase film was established on the GIC anode, markedly enhancing cycling stability compared to traditional metal K anodes. Notably, the use of a graphite-based anode not only mitigated side reactions triggered by oxygen crossover but also overcame the intrinsic limitations of metal anodes, such as excessive volume change and dendrite formation. This undergoes potassiation/depotassiation at a lower redox potential between 0.8 and 1.0 V (*vs.* K<sup>+/K</sup>), reaching a specific capacity around 110 mAh g<sup>-1</sup>. The experimental results demonstrated superior electrochemical performance and long-term stability, underscoring the effectiveness of the GIC anode approach.

## 4. Conclusion and outlook

K–O<sub>2</sub> batteries have attracted growing research interest due to the abundance of K metal, improved safety profile compared to Li–O<sub>2</sub> systems, and the potential for higher energy efficiency under idealized conditions. While theoretical projections suggest favourable performance, their practical implementation remains constrained by critical challenges such as limited cycle life, parasitic side reactions, and oxygen management. This review highlights recent advances in K–O<sub>2</sub> battery development, including progress in electrolytes, air cathodes, anodes, and solid-state electrolytes, with a focus on strategies to mitigate interfacial degradation and enhance long-term stability.

For example, high-donor solvents like DMSO have been shown to enhance O<sub>2</sub>/KO<sub>2</sub> redox kinetics and improve cycling stability compared to low-donor solvents like diglyme. While K–O<sub>2</sub> batteries can operate without bifunctional catalysts, rGO cathodes have demonstrated capacities exceeding 8.4 Ah g<sup>-1</sup> with good cycling stability (up to 200 cycles) and high round-trip efficiency. A thin, porous rGO cathode with a high surface area and pore volume facilitates efficient oxygen transport and KO<sub>2</sub> deposition, enabling superior ORR performance. To address safety concerns and prevent dendrite formation, alternative anodes such as K–Sb alloy, Na–K liquid alloy, BP-based liquid anodes and potassium-intercalated graphite have been explored. These materials have shown potential in suppressing dendritic growth, enhancing cycle life, and improving the rate capability of K–O<sub>2</sub> batteries. Though a significant advancement in this area has been made, continued research will be crucial for the practical implementation of K–O<sub>2</sub>.

Despite the promising advantages of K–O<sub>2</sub> batteries, several challenges remain, including limited cycling stability, dendritic growth, low specific energy and stability issues, which need to be investigated in depth.

i. Finding a suitable electrolyte with enhanced electrochemical stability could help mitigate side product formation and electrolyte consumption. Developing new electrolytes with high donor ability, such as ionic liquids or fluorinated solvents, can improve stability, suppress side reactions, and enhance oxygen solubility for better reaction kinetics.



Additionally, highly concentrated electrolytes<sup>102,103</sup> and localized highly concentrated electrolytes<sup>104</sup> could also be explored for K–O<sub>2</sub> batteries. While high-concentration electrolytes may improve stability, they also bring challenges such as increased viscosity and reduced ionic conductivity. These issues can be partially addressed using a localized high-concentration electrolyte with a co-solvent strategy. Striking the right balance is crucial for optimising battery performance.

ii. The superoxide-based K–O<sub>2</sub> batteries have demonstrated relatively high energy efficiencies even in the absence of electrocatalysts, highlighting their potential as next-generation energy storage systems. However, significant challenges remain before their practical application can be realized. Nevertheless, the risk to safety and significant side reactions associated with the K metal anode continue to impede its widespread commercialization. Additionally, K metal is prone to dendritic growth, causing short circuits and limiting cycle life. The reaction of K metal with an electrolyte further degrades the solid electrolyte interface, reducing coulombic efficiency and increasing overpotential. Other materials such as potassium–tin alloy, metal sulfides, and titanium-based anodes<sup>105</sup> should also be explored.

iii. The air cathode has received relatively less attention and requires further study, as it has been claimed that the cell can operate without a catalyst. One key issue is the passivation of the cathode surface due to KO<sub>2</sub> formation, which reduces discharge capacity and energy efficiency. Additionally, sluggish OER kinetics can contribute to low round-trip efficiency. Further research is also needed to better understand the kinetics of ORR/OER processes. Exploring high-surface-area carbon materials and metal oxides such as MnO<sub>2</sub>,<sup>55</sup> nickel oxides, titanium oxides<sup>106</sup> *etc.* could help address these challenges. Additional research is also needed to better understand the kinetics of ORR/OER processes.

iv. Oxygen crossover (diffusion of oxygen molecules from the cathode to the anode) and cathode–anode crosstalk (diffusion of reactive species from the cathode to the anode and *vice versa*), causing corrosion of K metal, are two of the significant challenges in K–O<sub>2</sub> batteries. To solve these issues, research should be carried out towards the development of membranes, or solid-state electrolytes, which allow the transport of only K<sup>+</sup> ions and block the other unwanted species. The application of these could improve the safety and cycling stability of the K–O<sub>2</sub> batteries.

v. K metal is highly reactive and has a lower melting point (63.5 °C), which increases the risk of thermal runaway in K metal-based batteries. Therefore, improved cell design and thermal management strategies should be investigated to mitigate the thermal runaway issue and improve the battery lifespan.

vi. Advanced characterization techniques, such as *in situ* XRD and XPS, play a crucial role in probing reaction mechanisms and guiding the design of novel materials. The prediction of electrode material properties can be effectively complemented by computational studies alongside experimental investigations, accelerating technological advancements. To

address the current challenges in K–O<sub>2</sub> batteries, future research should focus on stabilising discharge products and improving round-trip efficiency to enhance cycling performance. Strategies such as protective coatings or electrolyte additives can help mitigate side reactions, while optimising electrode structures and solvation environments can further enhance efficiency and stability. Ultimately, these advancements could pave the way for the practical adoption of K–O<sub>2</sub> batteries across various applications.

In summary, K–O<sub>2</sub> batteries are a very attractive option for high-energy applications, but they are still far from being a reality. Although some progress has been made, there is significant room for optimization, and much work remains before K–O<sub>2</sub> batteries can become a viable technology.

## Conflicts of interest

There are no conflicts to declare.

## Data availability

No new data have been created in this review article.

## Acknowledgements

ZK acknowledges J. Gust. Richert Stifftelse for project FunLig BAT (2024-00947) and the Swedish Electricity Storage and Balancing Centre (SESBC) project number MAT2023-21.

## References

- 1 N. Muradov and T. Veziroglu, *Int. J. Hydrogen Energy*, 2008, **33**, 6804–6839.
- 2 Z. Khan, T. R. Chetia, A. K. Vardhaman, D. Barpuzary, C. V. Sastri and M. Qureshi, *RSC Adv.*, 2012, **2**, 12122–12128.
- 3 Z. Khan, D. Kumar and X. Crispin, *Adv. Mater.*, 2023, **35**, 2300369.
- 4 Z. Khan, P. Singh, S. A. Ansari, S. R. Manippady, A. Jaiswal and M. Saxena, *Small*, 2021, **17**, e2006651.
- 5 K. V. Kravchyk, P. Bhauriyal, L. Piveteau, C. P. Guntlin, B. Pathak and M. V. Kovalenko, *Nat. Commun.*, 2018, **9**, 4469.
- 6 G. N. Lewis and F. G. Keyes, *J. Am. Chem. Soc.*, 1913, **35**, 340–344.
- 7 W. Xu, J. Wang, F. Ding, X. Chen, E. Nasybulin, Y. Zhang and J.-G. Zhang, *Energy Environ. Sci.*, 2014, **7**, 513–537.
- 8 Z. Khan, M. Vagin and X. Crispin, *Adv. Sci.*, 2020, **7**, 1902866.
- 9 V. Anoopkumar, B. John and M. Td, *ACS Appl. Energy Mater.*, 2020, **3**, 9478–9492.



- 10 C. Liu, M. Carboni, W. R. Brant, R. Pan, J. Hedman, J. Zhu, T. Gustafsson and R. Younesi, *ACS Appl. Mater. Interfaces*, 2018, **10**, 13534–13541.
- 11 J. Lu, L. Li, J.-B. Park, Y.-K. Sun, F. Wu and K. Amine, *Chem. Rev.*, 2014, **114**, 5611–5640.
- 12 D. Kumar, L. R. Franco, N. Abdou, R. Shu, A. Martinelli, C. M. Araujo, J. Gladisch, V. Gueskine, R. Crispin and Z. Khan, *Energy Environ. Mater.*, 2025, **8**, e12752.
- 13 Z. Khan, D. Kumar, S. Lander, J. Phopase and R. Crispin, *EcoEnergy*, 2024, **2**, 456–465.
- 14 J. Park, J.-Y. Hwang and W.-J. Kwak, *J. Phys. Chem. Lett.*, 2020, **11**, 7849–7856.
- 15 C. Wang, Y. Yu, J. Niu, Y. Liu, D. Bridges, X. Liu, J. Pooran, Y. Zhang and A. Hu, *Appl. Sci.*, 2019, **9**, 2787.
- 16 L. T. Hieu, S. So, I. T. Kim and J. Hur, *Chem. Eng. J.*, 2021, **411**, 128584.
- 17 J. Fu, Z. P. Cano, M. G. Park, A. Yu, M. Fowler and Z. Chen, *Adv. Mater.*, 2017, **29**, 1604685.
- 18 J. Zhou and S. Guo, *SmartMat*, 2021, **2**, 176–201.
- 19 G. Girishkumar, B. McCloskey, A. C. Luntz, S. Swanson and W. Wilcke, *J. Phys. Chem. Lett.*, 2010, **1**, 2193–2203.
- 20 F. Li, T. Zhang and H. Zhou, *Energy Environ. Sci.*, 2013, **6**, 1125–1141.
- 21 J. Xiao, D. Mei, X. Li, W. Xu, D. Wang, G. L. Graff, W. D. Bennett, Z. Nie, L. V. Saraf, I. A. Aksay, J. Liu and J.-G. Zhang, *Nano Lett.*, 2011, **11**, 5071–5078.
- 22 G. Houchins, V. Pande and V. Viswanathan, *ACS Energy Lett.*, 2020, **5**, 1893–1899.
- 23 A. Eftekhari, *J. Power Sources*, 2004, **126**, 221–228.
- 24 P. Hartmann, C. L. Bender, M. Vracar, A. K. Durr, A. Garsuch, J. Janek and P. Adelhelm, *Nat. Mater.*, 2013, **12**, 228–232.
- 25 X. Ren and Y. Wu, *J. Am. Chem. Soc.*, 2013, **135**, 2923–2926.
- 26 Y.-C. Lu, B. M. Gallant, D. G. Kwabi, J. R. Harding, R. R. Mitchell, M. S. Whittingham and Y. Shao-Horn, *Energy Environ. Sci.*, 2013, **6**, 750.
- 27 W.-J. Kwak, Rosy, D. Sharon, C. Xia, H. Kim, L. R. Johnson, P. G. Bruce, L. F. Nazar, Y.-K. Sun, A. A. Frimer, M. Noked, S. A. Freunberger and D. Aurbach, *Chem. Rev.*, 2020, **120**, 6626–6683.
- 28 R. Wang, J. Xue, Y. Zhao, R. Zheng and Y. Yang, *Acc. Mater. Res.*, 2021, **2**, 447–457.
- 29 X. Lin, Q. Sun, J. T. Kim, X. Li, J. Zhang and X. Sun, *Nano Energy*, 2023, **112**, 108466.
- 30 E. Mourad, Y. K. Petit, R. Spezia, A. Samojlov, F. F. Summa, C. Prehal, C. Leypold, N. Mahne, C. Slugovc, O. Fontaine, S. Brutti and S. A. Freunberger, *Energy Environ. Sci.*, 2019, **12**, 2559–2568.
- 31 L. Qin, H. Ao and Y. Wu, *Faraday Discuss.*, 2024, **248**, 60–74.
- 32 J. Sun, Y. Du, Y. Liu, D. Yan, X. Li, D. H. Kim, Z. Lin and X. Zhou, *Chem. Soc. Rev.*, 2025, **54**, 2543–2594.
- 33 J.-N. Liu, C.-X. Zhao, J. Wang, D. Ren, B.-Q. Li and Q. Zhang, *Energy Environ. Sci.*, 2022, **15**, 4542–4553.
- 34 A. G. Olabi, E. T. Sayed, T. Wilberforce, A. Jamal, A. H. Alami, K. Elsaid, S. M. A. Rahman, S. K. Shah and M. A. Abdelkareem, *Energies*, 2021, **14**, 7373.
- 35 P. G. Bruce, S. A. Freunberger, L. J. Hardwick and J.-M. Tarascon, *Nat. Mater.*, 2012, **11**, 19–29.
- 36 J. M. Munuera, J. I. Paredes, M. Enterría, S. Villar-Rodil, A. G. Kelly, Y. Nalawade, J. N. Coleman, T. Rojo, N. Ortiz-Vitoriano, A. Martínez-Alonso and J. M. D. Tascón, *ACS Appl. Mater. Interfaces*, 2020, **12**, 494–506.
- 37 L. Qin, L. Schkeryantz, J. Zheng, N. Xiao and Y. Wu, *J. Am. Chem. Soc.*, 2020, **142**, 11629–11640.
- 38 G. Vardar, J. G. Smith, T. Thompson, K. Inagaki, J. Naruse, H. Hiramatsu, A. E. S. Sleightholme, J. Sakamoto, D. J. Siegel and C. W. Monroe, *Chem. Mater.*, 2016, **28**, 7629–7637.
- 39 P. Reinsberg, C. J. Bondue and H. Baltruschat, *J. Phys. Chem. C*, 2016, **120**, 22179–22185.
- 40 M. A. Deyab and Q. Mohsen, *Renewable Sustainable Energy Rev.*, 2021, **139**, 110729.
- 41 J. Zhang, Q. Zhou, Y. Tang, L. Zhang and Y. Li, *Chem. Sci.*, 2019, **10**, 8924–8929.
- 42 W. Zhang, Y. Liu and Z. Guo, *Sci. Adv.*, 2019, **5**, eaav7412.
- 43 Y. Li and J. Lu, *ACS Energy Lett.*, 2017, **2**, 1370–1377.
- 44 H. W. Kim, V. J. Bukas, H. Park, S. Park, K. M. Diederichsen, J. Lim, Y. H. Cho, J. Kim, W. Kim, T. H. Han, J. Voss, A. C. Luntz and B. D. McCloskey, *ACS Catal.*, 2020, **10**, 852–863.
- 45 Z. Li, X. Yu, X. Wu, Y. Qiao and S. Ye, *J. Phys. Chem. C*, 2024, **128**, 17878–17885.
- 46 R. R. Kapaev, N. Leifer, A. R. Kottaichamy, A. Ohayon, L. Wu, M. Shalom and M. Noked, *Angew. Chem., Int. Ed.*, 2025, **64**, e202418792.
- 47 Z. Khan, U. Ail, F. Nadia Ajjan, J. Phopase, Z. Ullah Khan, N. Kim, J. Nilsson, O. Inganäs, M. Berggren and X. Crispin, *Adv. Energy Sustainability Res.*, 2022, **3**, 2100165.
- 48 B. Senthilkumar, Z. Khan, S. Park, I. Seo, H. Ko and Y. Kim, *J. Power Sources*, 2016, **311**, 29–34.
- 49 S. H. Sahgong, S. T. Senthilkumar, K. Kim, S. M. Hwang and Y. Kim, *Electrochem. Commun.*, 2015, **61**, 53–56.
- 50 F. Cheng and J. Chen, *Chem. Soc. Rev.*, 2012, **41**, 2172–2192.
- 51 Y. Wang, R. Yi, W. Fan, G. Li and Q. Yi, *J. Power Sources*, 2024, **624**, 235518.
- 52 Z. Khan, S. O. Park, J. Yang, S. Park, R. Shanker, H.-K. Song, Y. Kim, S. K. Kwak and H. Ko, *J. Mater. Chem. A*, 2018, **6**, 24459–24467.
- 53 S. Zhao, T. Liu, Y. Dai, J. Wang, Y. Wang, Z. Guo, J. Yu, I. T. Bello and M. Ni, *Appl. Catal., B*, 2023, **320**, 121992.
- 54 E. V. Timofeeva, C. U. Segre, G. S. Pour, M. Vazquez and B. L. Patawah, *Curr. Opin. Electrochem.*, 2023, **38**, 101246.
- 55 Z. Khan, S. Park, S. M. Hwang, J. Yang, Y. Lee, H.-K. Song, Y. Kim and H. Ko, *NPG Asia Mater.*, 2016, **8**, e294–e294.
- 56 Z. Khan, B. Senthilkumar, S. O. Park, S. Park, J. Yang, J. H. Lee, H.-K. Song, Y. Kim, S. K. Kwak and H. Ko, *J. Mater. Chem. A*, 2017, **5**, 2037–2044.
- 57 S. Y. Khan, T. Noor, N. Iqbal and Z. Ali, *Mater. Res. Bull.*, 2025, **183**, 113189.
- 58 J. Qian, Y. Chen, L. Wu, Y. Cao, X. Ai and H. Yang, *Chem. Commun.*, 2012, **48**, 7070–7072.



- 59 C. Zhou, X. Chen, S. Liu, Y. Han, H. Meng, Q. Jiang, S. Zhao, F. Wei, J. Sun, T. Tan and R. Zhang, *J. Am. Chem. Soc.*, 2022, **144**, 2694–2704.
- 60 N. Xiao, X. Ren, W. D. McCulloch, G. Gourdin and Y. Wu, *Acc. Chem. Res.*, 2018, **51**, 2335–2343.
- 61 P. Hartmann, C. L. Bender, M. Vračar, A. K. Dürr, A. Garsuch, J. Janek and P. Adelhelm, *Nat. Mater.*, 2013, **12**, 228–232.
- 62 Y. K. Petit, E. Mourad, C. Prehal, C. Leybold, A. Windischbacher, D. Mijailovic, C. Slugovc, S. M. Borisov, E. Zojer, S. Brutti, O. Fontaine and S. A. Freunberger, *Nat. Chem.*, 2021, **13**, 465–471.
- 63 X. Ren, K. C. Lau, M. Yu, X. Bi, E. Kreidler, L. A. Curtiss and Y. Wu, *ACS Appl. Mater. Interfaces*, 2014, **6**, 19299–19307.
- 64 N. Xiao, R. T. Rooney, A. A. Gewirth and Y. Wu, *Angew. Chem., Int. Ed.*, 2018, **57**, 1227–1231.
- 65 W. Wang, Y. Wang, C.-H. Wang, Y.-W. Yang and Y.-C. Lu, *Energy Storage Mater.*, 2021, **36**, 341–346.
- 66 Y. Qiao, H. Deng, Z. Chang, X. Cao, H. Yang and H. Zhou, *Natl. Sci. Rev.*, 2020, **8**, nwaa287.
- 67 N. Mahne, B. Schafzahl, C. Leybold, M. Leybold, S. Grumm, A. Leitgeb, G. A. Strohmeier, M. Wilkening, O. Fontaine, D. Kramer, C. Slugovc, S. M. Borisov and S. A. Freunberger, *Nat. Energy*, 2017, **2**, 17036.
- 68 J. Küpper and U. Simon, *Sustainable Energy Fuels*, 2022, **6**, 1992–2000.
- 69 J. Liu, L. Guo, Y. Xu, J. Huang and Z. Peng, *Faraday Discuss.*, 2024, **248**, 89–101.
- 70 L. Ni, G. Xu, C. Li and G. Cui, *Exploration*, 2022, **2**, 20210239.
- 71 S. Dhir, B. Jagger, A. Maguire and M. Pasta, *Nat. Commun.*, 2023, **14**, 3833.
- 72 M. Okoshi, Y. Yamada, S. Komaba, A. Yamada and H. Nakai, *J. Electrochem. Soc.*, 2017, **164**, A54.
- 73 C. Qiu, J. Jiang, X. Zhao, S. Chen, X. Ren and Y. Wu, *ACS Appl. Mater. Interfaces*, 2022, **14**, 55719–55726.
- 74 C. Xia, R. Black, R. Fernandes, B. Adams and L. F. Nazar, *Nat. Chem.*, 2015, **7**, 496–501.
- 75 N. Xiao, X. Ren, M. He, W. D. McCulloch and Y. Wu, *ACS Appl. Mater. Interfaces*, 2017, **9**, 4301–4308.
- 76 M. Zhou, P. Bai, X. Ji, J. Yang, C. Wang and Y. Xu, *Adv. Mater.*, 2021, **33**, 2003741.
- 77 H. Wang, J. Dong, Q. Guo, W. Xu, H. Zhang, K. C. Lau, Y. Wei, J. Hu, D. Zhai and F. Kang, *Energy Storage Mater.*, 2021, **42**, 526–532.
- 78 W. Wang and Y.-C. Lu, *Acc. Mater. Res.*, 2021, **2**, 515–525.
- 79 W. Wang, N.-C. Lai, Z. Liang, Y. Wang and Y.-C. Lu, *Angew. Chem., Int. Ed.*, 2018, **57**, 5042–5046.
- 80 P. Zhou, Y. Xiang and K. Liu, *Energy Environ. Sci.*, 2024, **17**, 8057–8077.
- 81 N. O. Vitoriano, I. Ruiz de Larramendi, R. L. Sacci, I. Lozano, C. A. Bridges, O. Arcelus, M. Enterría, J. Carrasco, T. Rojo and G. M. Veith, *Energy Storage Mater.*, 2020, **29**, 235–245.
- 82 S. Sankarasubramanian and V. Ramani, *J. Phys. Chem. C*, 2018, **122**, 19319–19327.
- 83 P. H. Reinsberg, A. Koellisch and H. Baltruschat, *Electrochim. Acta*, 2019, **313**, 223–234.
- 84 W. D. McCulloch, X. Ren, M. Yu, Z. Huang and Y. Wu, *ACS Appl. Mater. Interfaces*, 2015, **7**, 26158–26166.
- 85 X. Ren, M. He, N. Xiao, W. D. McCulloch and Y. Wu, *Adv. Energy Mater.*, 2017, **7**, 1601080.
- 86 W. Yu, K. C. Lau, Y. Lei, R. Liu, L. Qin, W. Yang, B. Li, L. A. Curtiss, D. Zhai and F. Kang, *ACS Appl. Mater. Interfaces*, 2017, **9**, 31871–31878.
- 87 G. Gourdin, N. Xiao, W. McCulloch and Y. Wu, *ACS Appl. Mater. Interfaces*, 2019, **11**, 2925–2934.
- 88 L. Qin, L. Schkeryantz and Y. Wu, *Angew. Chem., Int. Ed.*, 2023, **62**, e202213996.
- 89 J. Shao, H. Ao, L. Qin, J. Elgin, C. E. Moore, Y. Khalifa, S. Zhang and Y. Wu, *Adv. Mater.*, 2023, **35**, 2306809.
- 90 D.-C. Kong, M. Avdeev, L.-N. Song, L.-J. Zheng, X.-X. Wang and J.-J. Xu, *Energy Storage Mater.*, 2024, **72**, 103699.
- 91 X. Zhang, J. Wang, X. Lang, T. Wang, T. Qu, Q. Lai, L. Li, C. Yao and K. Cai, *J. Energy Storage*, 2024, **75**, 109590.
- 92 Y. Dou, Y. Zhang, F. Guo, Y. Shen, G. Chen, Y. Wei, Z. Xie and Z. Zhou, *Chem. Res. Chin. Univ.*, 2021, **37**, 254–258.
- 93 S. Singh, J. Küpper, A. Abouserie, G. Dalfollo, M. Noyong and U. Simon, *Batteries*, 2024, **10**, 192.
- 94 P. E. Mason, F. Uhlig, V. Vaněk, T. Buttersack, S. Bauerecker and P. Jungwirth, *Nat. Chem.*, 2015, **7**, 250–254.
- 95 C. Wei, Y. Tao, H. Fei, Y. An, Y. Tian, J. Feng and Y. Qian, *Energy Storage Mater.*, 2020, **30**, 206–227.
- 96 S. Komaba, T. Hasegawa, M. Dahbi and K. Kubota, *Electrochem. Commun.*, 2015, **60**, 172–175.
- 97 B. Horstmann, B. Gallant, R. Mitchell, W. G. Bessler, Y. Shao-Horn and M. Z. Bazant, *J. Phys. Chem. Lett.*, 2013, **4**, 4217–4222.
- 98 N. Ortiz-Vitoriano, T. P. Batcho, D. G. Kwabi, B. Han, N. Pour, K. P. C. Yao, C. V. Thompson and Y. Shao-Horn, *J. Phys. Chem. Lett.*, 2015, **6**, 2636–2643.
- 99 G. Cong, W. Wang, N.-C. Lai, Z. Liang and Y.-C. Lu, *Nat. Mater.*, 2019, **18**, 390–396.
- 100 L. Qin, S. Zhang, J. Zheng, Y. Lei, D. Zhai and Y. Wu, *Energy Environ. Sci.*, 2020, **13**, 3656–3662.
- 101 Y. Lei, Y. Chen, H. Wang, J. Hu, D. Han, J. Dong, W. Xu, X. Li, Y. Wang, Y. Wu, D. Zhai and F. Kang, *ACS Appl. Mater. Interfaces*, 2020, **12**, 37027–37033.
- 102 T. Hosaka, K. Kubota, H. Kojima and S. Komaba, *Chem. Commun.*, 2018, **54**, 8387–8390.
- 103 N. Ortiz-Vitoriano, I. R. de Larramendi, G. Àvall, R. Cid, M. Enterría, P. Johansson and R. Bouchal, *Energy Storage Mater.*, 2024, **70**, 103501.
- 104 P. Nie, M. Liu, W. Qu, M. Hou, L. Chang, Z. Wu, H. Wang and J. Jiang, *Adv. Funct. Mater.*, 2023, **33**, 2302235.
- 105 M. Ma, S. Chong, K. Yao, H. K. Liu, S. X. Dou and W. Huang, *Matter*, 2023, **6**, 3220–3273.
- 106 S. Karunarathne, C. K. Malaarachchi, A. M. Abdelkader and A. R. Kamali, *J. Power Sources*, 2024, **607**, 234553.

